

# 1 **A self-blinking DNA probe for live-cell superresolution 3D imaging of** 2 **hierarchical chromatin structures**

3 Yang Zheng<sup>1,2,9</sup>, Sen Ye<sup>1,9</sup>, Shumin Li<sup>3,9</sup>, Cuifang Liu<sup>4,5</sup>, Shihang Luo<sup>5,7</sup>, Yanqin Chen<sup>2</sup>, Yunsheng Li<sup>2</sup>,  
4 Lingyi Huang<sup>2</sup>, Shan Deng<sup>1</sup>, Ping Chen<sup>4,8</sup>, Yongdeng Zhang<sup>2</sup>, Wei Ji<sup>5,7</sup>, Ruibang Luo<sup>3</sup>, Guohong Li<sup>4,5,6\*</sup>  
5 & Dan Yang<sup>1,2\*</sup>

6 <sup>1</sup>Morningside Laboratory for Chemical Biology and Department of Chemistry, The University of Hong  
7 Kong, Hong Kong, China.

8 <sup>2</sup>School of Life Sciences, Westlake University, Hangzhou, Zhejiang, China.

9 <sup>3</sup>Department of Computer Science, The University of Hong Kong, Hong Kong, China.

10 <sup>4</sup>National Laboratory of Biomacromolecules, CAS Center for Excellence in Biomacromolecules,  
11 Institute of Biophysics, Chinese Academy of Sciences, Beijing, China.

12 <sup>5</sup>College of Life Science, University of Chinese Academy of Sciences, Beijing, China.

13 <sup>6</sup>Bioland Laboratory (Guangzhou Regenerative Medicine and Health Guangdong Laboratory),  
14 Guangzhou, Guangdong, China.

15 <sup>7</sup>Institute of Biophysics, Chinese Academy of Sciences, Beijing, China

16 <sup>8</sup>Department of Immunology, School of Basic Medical Sciences, Advanced Innovation Center for  
17 Human Brain Protection, Capital Medical University, Beijing, China.

18 <sup>9</sup>These authors contributed equally: Yang Zheng, Sen Ye, Shumin Li.

19 \*Correspondence: Guohong Li ([liguohong@ibp.ac.cn](mailto:liguohong@ibp.ac.cn)) or Dan Yang ([yangdan@westlake.edu.cn](mailto:yangdan@westlake.edu.cn))

20

## 21 **ABSTRACT**

22 How the 2-m-long genomic DNA is packaged into chromatin in the 10- $\mu$ m eukaryotic nucleus is a  
23 fundamental question in cell biology. DNA accessibility depends on chromatin structure and dynamics,  
24 which basically control all DNA-related processes, such as transcription, DNA replication and repair.

25 The hierarchical model of chromatin organization has been controversial in recent years because  
26 live-cell evidence for the existence of chromatin fibers, particularly those 30 nm in diameter, has  
27 remained elusive. Herein, we report a DNA-binding, fluorogenic and self-blinking small-molecule  
28 probe for the first live-cell 3D superresolution imaging of chromatin fibers with structural plasticity and  
29 fast dynamics. Selective inhibition of histone deacetylases led to decompaction of chromatin fibers due  
30 to hyperacetylation of histones. Our live-cell imaging results suggest a model of DNA packaging in  
31 interphase with the hierarchical organization of nucleosomal arrays and chromatin fibers.

## 32 INTRODUCTION

33 How the 2-m-long genomic DNA is packaged into the 10- $\mu$ m eukaryotic nucleus is a fundamental  
34 question. The classic model proposes that DNA is hierarchically packaged by histones into chromatin,  
35 which is organized into “beads-on-a-string” nucleosomal arrays, compact 30-nm chromatin fibers and  
36 even larger fibers beyond 30 nm in diameter<sup>1-3</sup>. DNA accessibility, controlled by dynamic chromatin  
37 organization, is critical for all DNA-dependent processes, including gene transcription and DNA  
38 replication and repair. However, the hierarchical model of chromatin organization has been  
39 controversial in recent years<sup>5-14</sup> due to the paucity of live-cell evidence for the existence of compact  
40 chromatin fibers, particularly those with a diameter of 30 nm. On the one hand, structures revealed *in*  
41 *vitro* do not necessarily represent native chromatin structures in living cells. Moreover, there are  
42 inevitable artifacts associated with *in vitro* approaches. For instance, the ChromEMT approach relies on  
43 a tedious and harsh sample preparation process of cell fixation, DRAQ5 staining, photooxidation and  
44 subsequent oxidative polymerization of diaminobenzidine (DAB), OsO<sub>4</sub> staining, EtOH dehydration and  
45 resin embedding<sup>12</sup>. What was stained by OsO<sub>4</sub> was not chromatin but the polymer of oxidized DAB. The  
46 native chromatin ultrastructure could have been damaged by photooxidation before electron microscopy  
47 (EM) analysis. On the other hand, live-cell superresolution microscopy approaches failed to reveal 3D  
48 chromatin structures with sufficient spatiotemporal resolution and labeling density<sup>10,11,13,15-18</sup>. Taken

49 together, these prior studies furnished only a limited understanding of chromatin structure and dynamics  
50 in living cells.

51 To address this puzzle, it is essential to develop a 3D superresolution imaging method for native  
52 chromatin structures in living cells with high spatiotemporal resolution and labeling density at modest  
53 laser intensity. For this purpose, a highly selective DNA-binding, self-blinking and fluorogenic probe,  
54 **6-HoeHESiR**, has been developed with its “ON” state population properly fine-tuned to quickly achieve  
55 high labeling density and minimize motion blur. This new probe has been validated by single-molecule  
56 localization microscopy (SMLM) with *in vitro* reconstituted nucleosomal arrays and 30-nm chromatin  
57 fibers, and our 3D imaging results are consistent with EM images. The 3D visualization of both  
58 nucleosomal arrays and chromatin fibers in living cells has been achieved with high spatiotemporal  
59 resolution and labeling density, even at reduced laser intensity for lower phototoxicity. We observed  
60 structural plasticity of chromatin fibers with 38- and 33-nm mean diameters in HeLa cells and chicken  
61 erythrocytes, respectively. Fast chromatin fiber dynamics were captured with less than 2-second  
62 temporal resolution, and the mean resting/dwelling lifetime of chromatin fibers in living HeLa cells was  
63 estimated to be 0.6 seconds. With this novel probe, we were able to observe the decompaction of  
64 chromatin fibers induced by small-molecule inhibitors of histone deacetylases (HDACs), providing the  
65 first live-cell evidence for the tight connection between the histone acetylation state and 3D chromatin  
66 organization with unprecedented resolution.

## 67 **RESULTS**

### 68 **The development of a DNA-binding, fluorogenic and self-blinking probe**

69 Superresolution fluorescence microscopy is a powerful tool for interrogating important biological  
70 questions. By bypassing the diffraction limit of light, superresolution microscopy has been developed to  
71 visualize previously unresolvable fine subcellular structures with nanometer-scale precision<sup>19-24</sup>. The  
72 commercial organic dyes (e.g., Alexa 647) widely used for SMLM still suffer from poor cell  
73 permeability and photoswitching buffers that are highly reducing and incompatible with live cells<sup>24</sup>.

74 Such limitations have impeded the study of important biological questions by live-cell SMLM. To  
75 overcome this bottleneck, we endeavor to develop new organic fluorophores with the following criteria:  
76 1) self-blinking with an absorption maximum in the deep red and near infrared regions to minimize  
77 autofluorescence and phototoxicity to living cells<sup>25</sup> and 2) a fine-tuned percentage of the fluorescent  
78 “ON” state for optimal localization number per frame to achieve sufficient labeling density in a short  
79 acquisition time while preventing signal overlap<sup>24</sup>. Urano group pioneered the self-blinking  
80 silicon-rhodamine fluorophore **HMSiR** for live-cell SMLM<sup>26</sup>. However, currently there has been no  
81 effort to fine-tune the self-blinking “ON” state population for optimal imaging quality and performance.  
82 Therefore, we rationally designed a new self-blinking Si-rhodamine fluorophore, **6-HESiR**, according  
83 to our design strategy (Fig. 1a-b). By replacing the hydroxymethyl group on the upper ring of **HMSiR**  
84 with a hydroxyethyl group<sup>26-28</sup>, the cyclization/ring opening self-blinking equilibrium is shifted toward  
85 the open, fluorescent “ON” state. This new fluorophore **6-HESiR** was successfully prepared with an  
86 efficient synthetic route (Supplementary Information, chemical synthesis section), and it could  
87 potentially increase the localization number per frame significantly for the fast acquisition of sufficient  
88 localizations to resolve dynamic fine structures. The “ON” state population of **6-HESiR** was found to be  
89 20% at physiological pH in aqueous buffer with **SiR650** as the benchmark of the 100% “ON” state (Fig.  
90 1b-d), and the  $pK_{cycl}$  value of **6-HESiR** was determined to be 6.6 (based on its pH titration curve, Fig. 1e;  
91 Supplementary Fig. 1a), higher than that of **HMSiR** ( $pK_{cycl} = 5.8$ , Fig. 1a).  
92 The successful implementation of live-cell SMLM hinges not only on the self-blinking fluorophore but  
93 also on a fully biocompatible labeling strategy that is noninvasive, highly selective, and artifact-free  
94 with high labeling density. In this regard, we chose the Hoechst tagging strategy, as it has found some  
95 success in developing fluorogenic probes for live-cell chromatin imaging<sup>13,16,17,29-31</sup> with low  
96 cytotoxicity. The Hoechst moiety could perform highly selective noncovalent binding to the DNA minor  
97 groove with negligible linkage error between the target DNA molecule and our novel self-blinking dye  
98 **6-HESiR**. Therefore, we designed and synthesized **6-HoeHESiR** by connecting **6-HESiR** and the

99 Hoechst fragment with a carbamate linker (Fig. 2a). The *in vitro* binding of **6-HoeHESiR** to a  
100 benchmark hairpin DNA (hpDNA) molecule (Fig. 2b) with an AATT Hoechst binding site<sup>32</sup> was  
101 studied by fluorescence titration. In the absence of hpDNA, the fluorescence of **6-HoeHESiR** was  
102 nearly quenched (Fig. 2c). A dose-dependent fluorescence turn-on was observed upon the addition of  
103 increasing equivalents of hpDNA to **6-HoeHESiR** (Fig. 2c). A 43-fold fluorescence increase with 14  
104  $\mu\text{M}$  of hpDNA confirmed the sensitivity and fluorogenicity of **6-HoeHESiR**. Based on the titration  
105 curve, the dissociation constant ( $K_D$ ) of the complex formed by **6-HoeHESiR** and hpDNA was  
106 estimated to be 3.8  $\mu\text{M}$ . Attachment of **6-HESiR** to the Hoechst dye caused a slight redshift of both the  
107 absorbance and fluorescence maxima of **6-HoeHESiR**. Upon the addition of hpDNA (14  $\mu\text{M}$ ), the  
108 absorbance of **6-HoeHESiR** was increased to a level close to that of the free fluorophore **6-HESiR**  
109 (Supplementary Fig. 2a), and the fluorescence of **6-HoeHESiR** was recovered to 21% of that of  
110 **6-HESiR** (Fig. 2d).

#### 111 **SMLM with *in vitro* lambda DNA and reconstituted chromatin structures**

112 To evaluate our new probe **6-HoeHESiR**, we first attempted an SMLM experiment of spin-coated  
113 lambda DNA<sup>33</sup> with (A/T)<sub>4</sub> binding sites for the Hoechst moiety<sup>32</sup>. A full width at half maximum  
114 (FWHM) of 26 nm was successfully obtained (Supplementary Fig. 3), within the range of 20–30 nm as  
115 reported in literature. Then, we focused on *in vitro* reconstituted nucleosomal arrays and 30-nm  
116 chromatin fibers as benchmarks well characterized by EM<sup>34</sup> (Fig. 3d and 3g; Supplementary Fig. 4a and  
117 4e). Apart from the AATT binding site, three additional Hoechst binding sites<sup>32</sup> in the DNA template for  
118 *in vitro* reconstituted chromatin samples were also identified by fluorescence titration (Fig. 3a and 3b;  
119 Supplementary Fig. 2b-d). Based on the dissociation constants, the half-life of the complex formed by  
120 **6-HoeHESiR** and a nucleosome was estimated to be 10-20 ms<sup>32</sup>. Thus, fast binding/dissociation cycles  
121 between **6-HoeHESiR** and nucleosomes could allow fast self-blinking with a pool of **6-HoeHESiR**  
122 molecules in the unbound state (Fig. 2e). Since the hydrophobic environment in the nucleus favors the  
123 closed "OFF" state<sup>27</sup> (Fig. 1b) and the open form of **6-HoeHESiR** in the unbound state is nearly

124 quenched in fluorescence (Fig. 2c), the "ON" state population of **6-HoeHESiR** in chromatin imaging is  
125 expected to be lower than the 20% "ON" fraction of **6-HESiR** measured in aqueous buffer. Gratifyingly,  
126 **6-HoeHESiR** exhibited excellent self-blinking in SMLM experiments on reconstituted chromatin  
127 samples at a modest laser intensity<sup>25</sup> of 950 W/cm<sup>2</sup> (Supplementary Video 1). The reconstituted  
128 nucleosomal arrays displayed the pattern of discrete fluorescence signals (Fig. 3c and 3e;  
129 Supplementary Fig. 4b), which resembles the EM images (Fig. 3d; Supplementary Fig. 4a). Analysis of  
130 localizations on individual nucleosomes indicated that the ratio of axial to lateral resolution is 2.3  
131 (Supplementary Fig. 4c and 4d). To extract 3D structural features of reconstituted 30-nm chromatin  
132 fibers visualized in 3D SMLM experiments (Fig. 3f and 3h; Supplementary Fig. 4f), we developed an  
133 image analysis framework/program (Supplementary Information, image analysis section). Statistical  
134 results showed that the reconstituted chromatin fibers had a mean diameter of 33 nm, length of 114 nm,  
135 mean localization precision of 7.8 nm and labeling density of 32,944 molecules/ $\mu\text{m}^3$  (Supplementary  
136 Fig. 4g; Supplementary Video 2 and 3). Although the reconstituted 30-nm fibers without biotin labels  
137 were visualized by EM in a dry and flattened state (Supplementary Information, EM analysis section),  
138 unlike our 3D SMLM approach, the 3D structural features obtained with **6-HoeHESiR** were consistent  
139 with those revealed by EM (Fig. 3h and 3i). Some elongated fibers were observed, probably due to  
140 slight loosening in the aqueous buffer (without glutaldehyde as a crosslinker) compared with the dry  
141 state in EM analysis.

## 142 **Hierarchical chromatin structures in living cells**

143 Building upon the solid validation of **6-HoeHESiR** with benchmark *in vitro* reconstituted nucleosomal  
144 arrays and 30-nm chromatin fibers, we then attempted to image native chromatin structures in living  
145 cells. First, we optimized the incubation conditions of **6-HoeHESiR** with living HeLa cells by  
146 light-sheet microscopy (Fig. 4a and 4b; Supplementary Fig. 5a and 5b). To our delight, **6-HoeHESiR**  
147 exhibited good cell permeability and high selectivity to provide 3D visualization of chromatin structures  
148 in whole nuclei. Without the Hoechst fragment, **6-HESiR** did not stain any nuclear component

149 (Supplementary Fig. 5c). Cytotoxicity assay showed that **6-HoeHESiR** caused negligible toxicity with a  
150 short incubation time (Supplementary Fig. 5d). Subsequent 3D SMLM experiments showed that  
151 **6-HoeHESiR** maintained its excellent self-blinking capacity in living HeLa cells (Supplementary Video  
152 4), and chromatin structures were clearly revealed (Fig. 4c; Supplementary Fig. 6a). Based on the  
153 structural resemblance to *in vitro* reconstituted benchmark chromatin samples, we identified two  
154 categories of chromatin structures in living HeLa cells. The first category consists of nucleosomal arrays  
155 (Fig. 4d), which displayed the same pattern of discrete fluorescence signals (Fig. 3d and 3e). The second  
156 category consists of chromatin fibers (Fig. 4e; Supplementary Fig. 6b). With the aid of the same image  
157 analysis program, these fibers were identified with a mean localization precision of 7.5 nm, short and  
158 long fiber diameters of 33 and 44 nm, and a labeling density of 32,996 molecules/ $\mu\text{m}^3$  (Fig. 4f;  
159 Supplementary Fig. 6c; Supplementary Video 5 and 6). The statistical distribution of 3D sizes and  
160 long-to-short fiber diameter ratios and the heterogeneity of structural characteristics could reflect the  
161 structural plasticity/polymorphism of chromatin fibers involved in highly sophisticated biological  
162 functions<sup>1-3</sup>. Our 2D imaging results are consistent with recent reports<sup>10,11,13</sup> that nucleosome clutches or  
163 chromatin domains were observed with no clear evidence of horizontally or randomly oriented  
164 chromatin fibers. However, our 3D analysis, performed both manually and by the computer program,  
165 identified chromatin fibers oriented axially or slightly tilted from the vertical axis. We propose that such  
166 an ordered chromatin fiber orientation might not only be consistent with highly regulated replication and  
167 transcription processes but facilitate these processes. The overlay of widefield images showed that the  
168 chromatin fibers reside in both the peripheral and the interior regions of the nuclei (Fig. 4g;  
169 Supplementary Fig. 6d). Remarkably, chromatin structures in the nucleus are quite dynamic  
170 (Supplementary Video 7). We were able to capture transient chromatin fibers with a temporal resolution  
171 of less than 2 seconds (Fig. 4h; Supplementary Video 8). The mean resting/residing lifetime of  
172 chromatin fibers was estimated to be 0.6 seconds (Supplementary Fig. 6e), implying fast-turnover  
173 transitions that are consistent with fast transcription activities. This dwelling lifetime is comparable to

174 the time scale of folding and unfolding dynamics of *in vitro*-reconstituted 30-nm chromatin fibers  
175 revealed by single-molecule force spectroscopy<sup>34</sup>. The structural plasticity and fast dynamics of  
176 chromatin fibers might be closely associated with complex regulatory factors, including histone variants  
177 and modifications, chromatin remodelers, and histone chaperons<sup>1-3</sup>, for the regulation of DNA  
178 accessibility and activities. When the laser intensity was reduced to a modest level of 950 W/cm<sup>2</sup> from  
179 3.2 kW/cm<sup>2</sup> to alleviate phototoxicity, nucleosomal arrays were visualized again, and we could still  
180 identify chromatin fibers at sufficient resolution with a mean localization precision of 8.8 nm, short and  
181 long fiber diameters of 33 and 42 nm, and a labeling density of 29,436 molecules/μm<sup>3</sup> (Supplementary  
182 Fig. 7a-f). Fast chromatin dynamics were also revealed, and the mean resting lifetime of chromatin  
183 fibers was estimated to be 0.6 seconds (Supplementary Video 9; Supplementary Fig. 7g), similar to the  
184 result obtained under 3.2 kW/cm<sup>2</sup> laser intensity.

185 A previous cryo-electron tomography (cryo-ET) study identified short chromatin fibers with 30 nm in  
186 diameter in isolated nuclei from chicken erythrocytes<sup>7</sup>. Therefore, we also attempted 3D SMLM  
187 experiments on living chicken erythrocytes with **6-HoeHESiR**. By applying a modest laser intensity of  
188 950 W/cm<sup>2</sup>, 3D chromatin structures in chicken erythrocyte nuclei were successfully visualized (Fig.  
189 5a-c; Supplementary Fig. 8a; Supplementary Video 10). The same two categories of chromatin  
190 structures were observed, and chromatin fibers were identified with a mean localization precision of 8  
191 nm, short and long fiber diameters of 29 and 37 nm, and a higher labeling density of 56,359  
192 molecules/μm<sup>3</sup> (Fig. 5d-g; Supplementary Fig. 8b-d; Supplementary Video 11 and 12). The fast  
193 dynamics of chromatin structures in chicken erythrocyte nuclei were also observed (Supplementary  
194 Video 13), with the mean resting lifetime of chromatin fibers estimated to be 1 second (Supplementary  
195 Fig. 8e).

### 196 **The connection between 3D chromatin organization and histone acetylation**

197 A previous study showed that histone acetylation is a critical epigenetic marker for chromatin fiber  
198 relaxation and optimal transcription, while deacetylation is required for chromatin fiber condensation



199 and transcriptional repression<sup>35</sup>. Histone deacetylases (HDACs), key enzymes that modulate acetylation,  
200 can be important drug targets to counteract abnormal protein acetylation status, induce chromatin  
201 decompaction, and reactivate tumor suppressor genes<sup>36,37</sup>. To investigate the connection between  
202 chromatin fibers and histone acetylation in living cells, we selected three HDAC inhibitors (Fig. 6a): 1)  
203 trichostatin A (TSA), a widely used HDAC pan-inhibitor; 2) entinostat, a class I HDAC 1–3 selective  
204 inhibitor; and 3) ricolinostat, a class IIb HDAC 6 selective inhibitor. Live HeLa cells were treated with  
205 these HDAC inhibitors and then imaged by 3D SMLM (Fig. 6b). The results showed that the density of  
206 chromatin fibers decreased by 52% and 63% upon TSA and entinostat treatments, respectively (Fig. 6c  
207 and 6d; Supplementary Fig. 9 and 10). However, no significant change in fiber density was observed  
208 upon ricolinostat treatment (Fig. 6c and 6d; Supplementary Fig. 11). Both the nonselective inhibition of  
209 HDACs and the selective inhibition of class I HDACs 1–3 led to decompaction of chromatin fibers<sup>38,39</sup>.  
210 In contrast, selective inhibition of class IIb HDAC 6 induced no significant fiber decompaction. These  
211 results are consistent with the literature reports that the functions of class I HDACs 1–3 are exclusively  
212 restricted to the nucleus, while class IIb HDAC 6 functions largely outside the nucleus by mediating the  
213 deacetylation of cytosolic proteins<sup>40</sup>. Taken together, our live-cell 3D imaging results provide new  
214 insights into the global change in 3D chromatin organization in response to histone hyperacetylation  
215 induced by small-molecule HDAC inhibitors.

## 216 **DISCUSSION**

217 Our findings allow us to depict genomic DNA packaging through the dynamic organization of  
218 nucleosomal arrays and chromatin fibers in living cells (Fig. 7). To the best of our knowledge, our 3D  
219 imaging results have furnished the first live-cell evidence for a hierarchical model of dynamic chromatin  
220 organization. We propose that nucleosomal arrays could be regarded as the primary chromatin structures  
221 and chromatin fibers as the secondary and higher-order structures. The structural  
222 plasticity/heterogeneity and fast dynamics of chromatin fibers are consistent with the complex

223 regulatory environment in the nucleus, such as histone modifications and variants, nonhistone  
224 architectural proteins, and linker DNA lengths for various biological functions<sup>1-3</sup>. The  
225 density/population of chromatin fibers was reduced by small-molecule inhibitors of HDACs that are  
226 responsible for histone deacetylation. For the first time, this phenomenon provides a live-cell 3D view  
227 of the tight connection between the histone acetylation state and chromatin hierarchical organization  
228 with unprecedented resolution.

229 The linchpin of our success is the new self-blinking fluorogenic probe, **6-HoeHESiR**, developed  
230 according to our new design strategy to increase the self-blinking “ON” state population to a suitable  
231 level. This design strategy has resulted in high spatiotemporal resolution and labeling density even at a  
232 moderate laser intensity for reduced phototoxicity. In light of our initial success, we envision that our  
233 new design strategy could be implemented to develop more self-blinking fluorophores and probes to  
234 enable the study of subcellular organelles and biological events by live-cell 3D superresolution imaging.

## 235 **Acknowledgments**

236 We thank the HKU Li Ka Shing Faculty of Medicine Imaging and the Flow Cytometry Core of CPOS  
237 for support in cell imaging. This work was supported by The University of Hong Kong, Westlake  
238 University, Morningside Foundation, and Hong Kong Research Grants Council under the Area of  
239 Excellence Scheme (AoE/P-705/16 to D.Y.). This work was supported by grants for G.L. from the  
240 National Natural Science Foundation of China (31991161), the Ministry of Science and Technology of  
241 China (2017YFA0504202), the Beijing Municipal Science and Technology Commission  
242 (Z201100005320013) and the HHMI International Research Scholars Program (55008737). R. L. was  
243 supported by the ECS (grant number 27204518) of the Hong Kong SAR government and by the URC  
244 fund at the University of Hong Kong. We thank Dr. Teng Zhao and Dr. Zhe Hu for their technical  
245 support in light-sheet microscopy. We thank Dr. Zhe Hu, Dr. Teng Zhao, Dr. Shengwang Du and Dr.  
246 Wei Li for helpful discussions. We thank Dr. Nai-Kei Wong and Ms. Jasmine Chit Ying Lau for  
247 proofreading the manuscript.

248 **Author contributions**

249 Y.Z., G.L. and D.Y. conceived the project. G.L. and D.Y. supervised and directed the research. Y.Z.  
250 designed and synthesized **6-HESiR** and **6-HoeHESiR**. Y.Z. studied photophysical properties with  
251 contributions from S.Y. C.L. prepared *in vitro*-reconstituted samples and performed electron  
252 microscopy analysis. S.-H.L. performed the SMLM experiment with lambda DNA and analyzed the  
253 data. Y.Z., S.Y. and S.D. performed cell culture and treatment. Y.Z. and S.Y. performed SMLM  
254 experiments with reconstituted chromatin structures and living cells. Y.C. and Y.L. performed the  
255 SMLM validation experiments. L.H. performed cytotoxicity assay. S.-M.L. developed the computer  
256 program and the web server for chromatin fiber analysis under the supervision of R.L. Y.Z. analyzed  
257 chromatin imaging data and performed statistical analysis with contributions from S.Y. and S.-M.L.  
258 Y.Z., S.Y., G.L. and D.Y. interpreted imaging results with contributions from all other authors. Y.Z.,  
259 S.Y., G.L. and D.Y. wrote the manuscript with input from all other authors.

260 **Competing interests**

261 The authors declare no competing interests.

262 **Data availability**

263 All data that support the findings of this manuscript are provided in text, figures, and supplementary  
264 videos. Original data are provided upon reasonable request to the correspondence authors.

265

266 **REFERENCES**

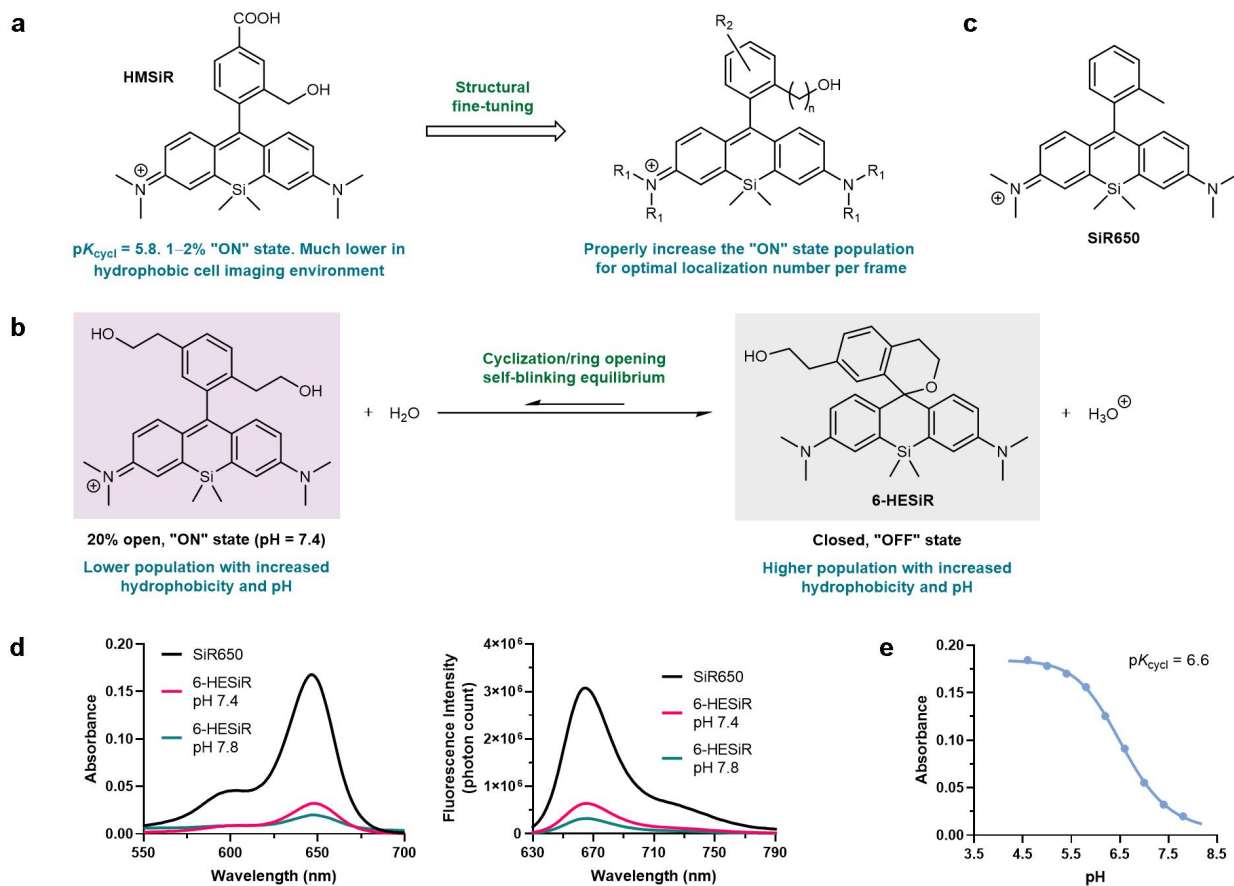
- 267 1. Li, G. & Reinberg, D. Chromatin higher-order structures and gene regulation. *Curr. Opin. Genet.*  
268 *Dev.* **21**, 175-186 (2011).
- 269 2. Luger, K., Dechassa, M. L. & Tremethick, D. J. New insights into nucleosome and chromatin  
270 structure: an ordered state or a disordered affair? *Nat. Rev. Mol. Cell Biol.* **13**, 436-447 (2012).

- 271 3. Chen, P., Li, W. & Li, G. Structures and Functions of Chromatin Fibers. *Annual Review of*  
272 *Biophysics* **50**, 95-116 (2021).
- 273 4. Luger, K., Mäder, A. W., Richmond, R. K., Sargent, D. F. & Richmond, T. J. Crystal structure of  
274 the nucleosome core particle at 2.8 Å resolution. *Nature* **389**, 251-260 (1997).
- 275 5. Schalch, T., Duda, S., Sargent, D. F. & Richmond, T. J. X-ray structure of a tetranucleosome and  
276 its implications for the chromatin fibre. *Nature* **436**, 138-141 (2005).
- 277 6. Song, F. *et al.* Cryo-EM Study of the Chromatin Fiber Reveals a Double Helix Twisted by  
278 Tetranucleosomal Units. *Science* **344**, 376-380 (2014).
- 279 7. Scheffer, M. P., Eltsov, M. & Frangakis, A. S. Evidence for short-range helical order in the 30-nm  
280 chromatin fibers of erythrocyte nuclei. *Proc. Natl. Acad. Sci. U.S.A.* **108**, 16992-16997 (2011).
- 281 8. Risca, V. I., Denny, S. K., Straight, A. F. & Greenleaf, W. J. Variable chromatin structure revealed  
282 by in situ spatially correlated DNA cleavage mapping. *Nature* **541**, 237-241 (2017).
- 283 9. Hsieh, T.-H. S. *et al.* Resolving the 3D Landscape of Transcription-Linked Mammalian Chromatin  
284 Folding. *Molecular Cell* **78**, 539-553.e538 (2020).
- 285 10. Ricci, Maria A., Manzo, C., García-Parajo, M. F., Lakadamyali, M. & Cosma, Maria P. Chromatin  
286 Fibers Are Formed by Heterogeneous Groups of Nucleosomes In Vivo. *Cell* **160**, 1145-1158  
287 (2015).
- 288 11. Nozaki, T. *et al.* Dynamic Organization of Chromatin Domains Revealed by Super-Resolution  
289 Live-Cell Imaging. *Mol. Cell* **67**, 282-293 (2017).
- 290 12. Ou, H. D. *et al.* ChromEMT: Visualizing 3D chromatin structure and compaction in interphase and  
291 mitotic cells. *Science* **357**, eaag0025 (2017).
- 292 13. Bucevičius, J., Gilat, T. & Lukinavičius, G. Far-red switching DNA probes for live cell nanoscopy.  
293 *Chem. Commun.* **56**, 14797-14800 (2020).
- 294 14. Lakadamyali, M. & Cosma, M. P. Visualizing the genome in high resolution challenges our  
295 textbook understanding. *Nat. Methods* **17**, 371-379 (2020).

- 296 15. Wombacher, R. *et al.* Live-cell super-resolution imaging with trimethoprim conjugates. *Nat.*  
297 *Methods* **7**, 717-719 (2010).
- 298 16. Bucevičius, J., Keller-Findeisen, J., Gilat, T., Hell, S. W. & Lukinavičius, G. Rhodamine–Hoechst  
299 positional isomers for highly efficient staining of heterochromatin. *Chem. Sci.* **10**, 1962-1970  
300 (2019).
- 301 17. Bucevičius, J., Kostiuk, G., Gerasimaitė, R., Gilat, T. & Lukinavičius, G. Enhancing the  
302 biocompatibility of rhodamine fluorescent probes by a neighbouring group effect. *Chem. Sci.* **11**,  
303 7313-7323 (2020).
- 304 18. Chi, W. *et al.* Descriptor  $\Delta$ GC-O Enables the Quantitative Design of Spontaneously Blinking  
305 Rhodamines for Live-Cell Super-Resolution Imaging. *Angew. Chem. Int. Ed.* **59**, 20215-20223  
306 (2020).
- 307 19. Liu, Z., Lavis, Luke D. & Betzig, E. Imaging Live-Cell Dynamics and Structure at the  
308 Single-Molecule Level. *Mol. Cell* **58**, 644-659 (2015).
- 309 20. Sauer, M. & Heilemann, M. Single-Molecule Localization Microscopy in Eukaryotes. *Chem. Rev.*  
310 **117**, 7478-7509 (2017).
- 311 21. von Diezmann, A., Shechtman, Y. & Moerner, W. E. Three-Dimensional Localization of Single  
312 Molecules for Super-Resolution Imaging and Single-Particle Tracking. *Chem. Rev.* **117**,  
313 7244-7275 (2017).
- 314 22. Sahl, S. J., Hell, S. W. & Jakobs, S. Fluorescence nanoscopy in cell biology. *Nat. Rev. Mol. Cell*  
315 *Biol.* **18**, 685-701 (2017).
- 316 23. Sigal, Y. M., Zhou, R. & Zhuang, X. Visualizing and discovering cellular structures with  
317 super-resolution microscopy. *Science* **361**, 880-887 (2018).
- 318 24. Lelek, M. *et al.* Single-molecule localization microscopy. *Nat. Rev. Methods Primers* **1**, 39,  
319 (2021).

- 320 25. Wäldchen, S., Lehmann, J., Klein, T., van de Linde, S. & Sauer, M. Light-induced cell damage in  
321 live-cell super-resolution microscopy. *Sci. Rep.* **5**, 15348 (2015).
- 322 26. Uno, S.-n. *et al.* A spontaneously blinking fluorophore based on intramolecular spirocyclization  
323 for live-cell super-resolution imaging. *Nat. Chem.* **6**, 681-689 (2014).
- 324 27. Takakura, H. *et al.* Long time-lapse nanoscopy with spontaneously blinking membrane probes. *Nat.*  
325 *Biotechnol.* **35**, 773-780 (2017).
- 326 28. Uno, S.-n., Kamiya, M., Morozumi, A. & Urano, Y. A green-light-emitting, spontaneously  
327 blinking fluorophore based on intramolecular spirocyclization for dual-colour super-resolution  
328 imaging. *Chem. Commun.* **54**, 102-105 (2018).
- 329 29. Nakamura, A. *et al.* Hoechst tagging: a modular strategy to design synthetic fluorescent probes for  
330 live-cell nucleus imaging. *Chem. Commun.* **50**, 6149-6152 (2014).
- 331 30. Lukinavičius, G. *et al.* SiR–Hoechst is a far-red DNA stain for live-cell nanoscopy. *Nat. Commun.*  
332 **6**, 8497 (2015).
- 333 31. Zhang, X. *et al.* A targetable fluorescent probe for dSTORM super-resolution imaging of live cell  
334 nucleus DNA. *Chem. Commun.* **55**, 1951-1954 (2019).
- 335 32. Breusegem, S. Y., Clegg, R. M. & Loontjens, F. G. Base-sequence specificity of Hoechst 33258  
336 and DAPI binding to five (A/T)<sub>4</sub> DNA sites with kinetic evidence for more than one high-affinity  
337 Hoechst 33258-AATT complex. *J. Mol. Biol.* **315**, 1049-1061 (2002).
- 338 33. Zhang, Y. *et al.* Ultrafast, accurate, and robust localization of anisotropic dipoles. *Protein & Cell* **4**,  
339 598-606 (2013).
- 340 34. Li, W. *et al.* FACT Remodels the Tetranucleosomal Unit of Chromatin Fibers for Gene  
341 Transcription. *Mol. Cell* **64**, 120-133 (2016).
- 342 35. Li, G. *et al.* Highly Compacted Chromatin Formed In Vitro Reflects the Dynamics of  
343 Transcription Activation In Vivo. *Mol. Cell* **38**, 41-53 (2010).

- 344 36. Li, Y. & Seto, E. HDACs and HDAC Inhibitors in Cancer Development and Therapy. *Cold Spring*  
345 *Harb. Perspect. Med.* **6**, a026831 (2016).
- 346 37. Eckschlager, T., Plch, J., Stiborova, M. & Hrabeta, J. Histone Deacetylase Inhibitors as Anticancer  
347 Drugs. *Int. J. Mol. Sci.* **18**, 1414 (2017).
- 348 38. Tóth, K. F. *et al.* Trichostatin A-induced histone acetylation causes decondensation of interphase  
349 chromatin. *J. Cell Sci.* **117**, 4277-4287 (2004).
- 350 39. Otterstrom, J. *et al.* Super-resolution microscopy reveals how histone tail acetylation affects DNA  
351 compaction within nucleosomes in vivo. *Nucleic Acids Res.* **47**, 8470-8484 (2019).
- 352 40. Fallah, M. S., Szarics, D., Robson, C. M. & Eubanks, J. H. Impaired Regulation of Histone  
353 Methylation and Acetylation Underlies Specific Neurodevelopmental Disorders. *Front. Genet.* **11**,  
354 613098 (2021).
- 355



356

357 **Fig. 1 Development of 6-HESiR. a**, New design principle of developing self-blinking fluorophores. **B**,

358 Self-blinking mechanism. **C**, Structure of **SiR650**. **D**, Absorption and fluorescence emission spectra of

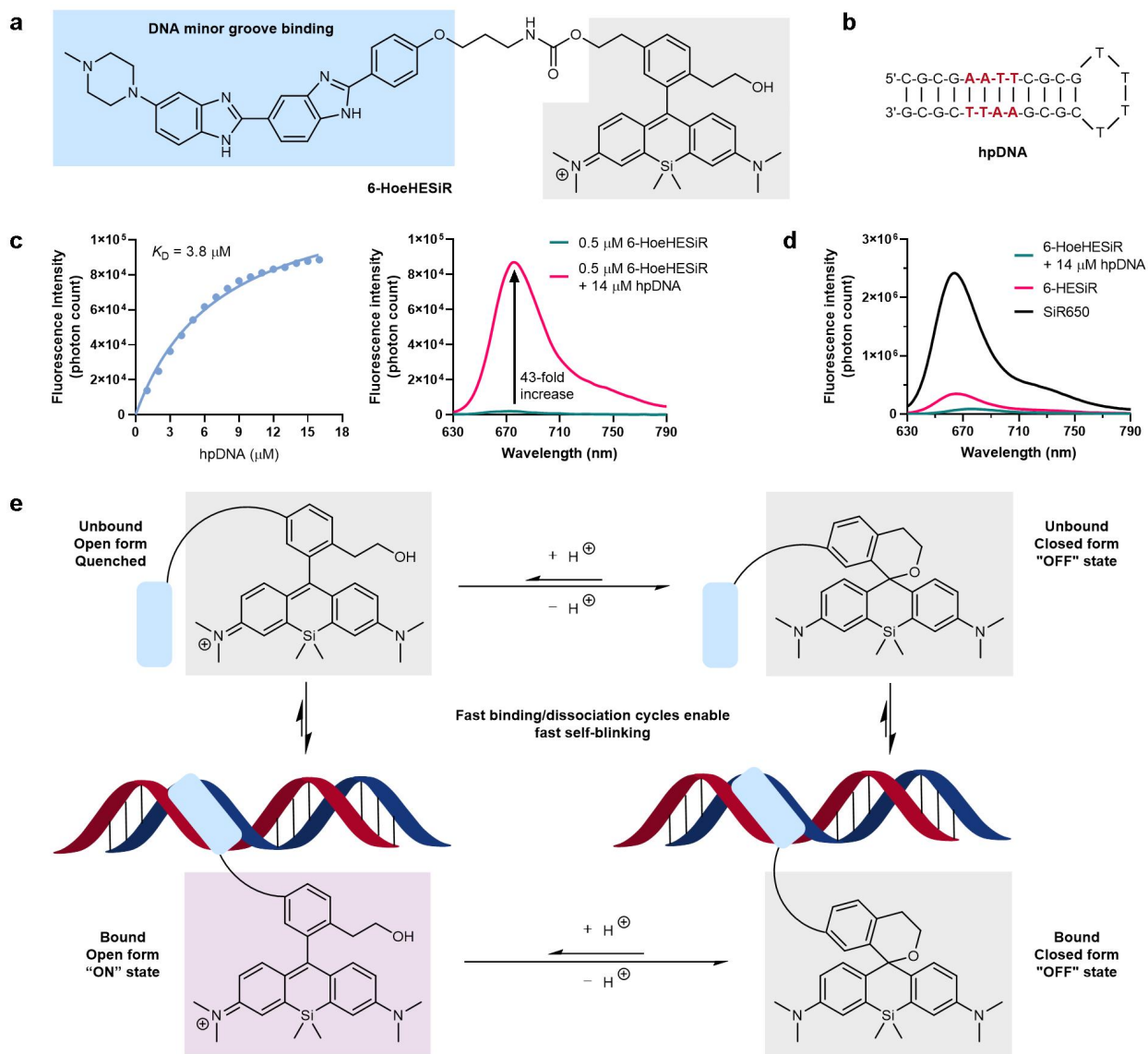
359 **6-HESiR** (2  $\mu$ M) in 0.1 M potassium phosphate buffer (pH = 7.4 and 7.8) with **SiR650** (2  $\mu$ M) as the

360 "100%" benchmark. Abs<sub>max</sub> at 648 nm. Fl<sub>max</sub> at 665 nm. **E**, pH titration of **6-HESiR** (2  $\mu$ M) in 0.1 M

361 potassium phosphate buffer.

362





363

364 **Fig. 2 Development of 6-HoeHESiR. a**, Rational design of 6-HoeHESiR. **b**, Structure of the hpDNA

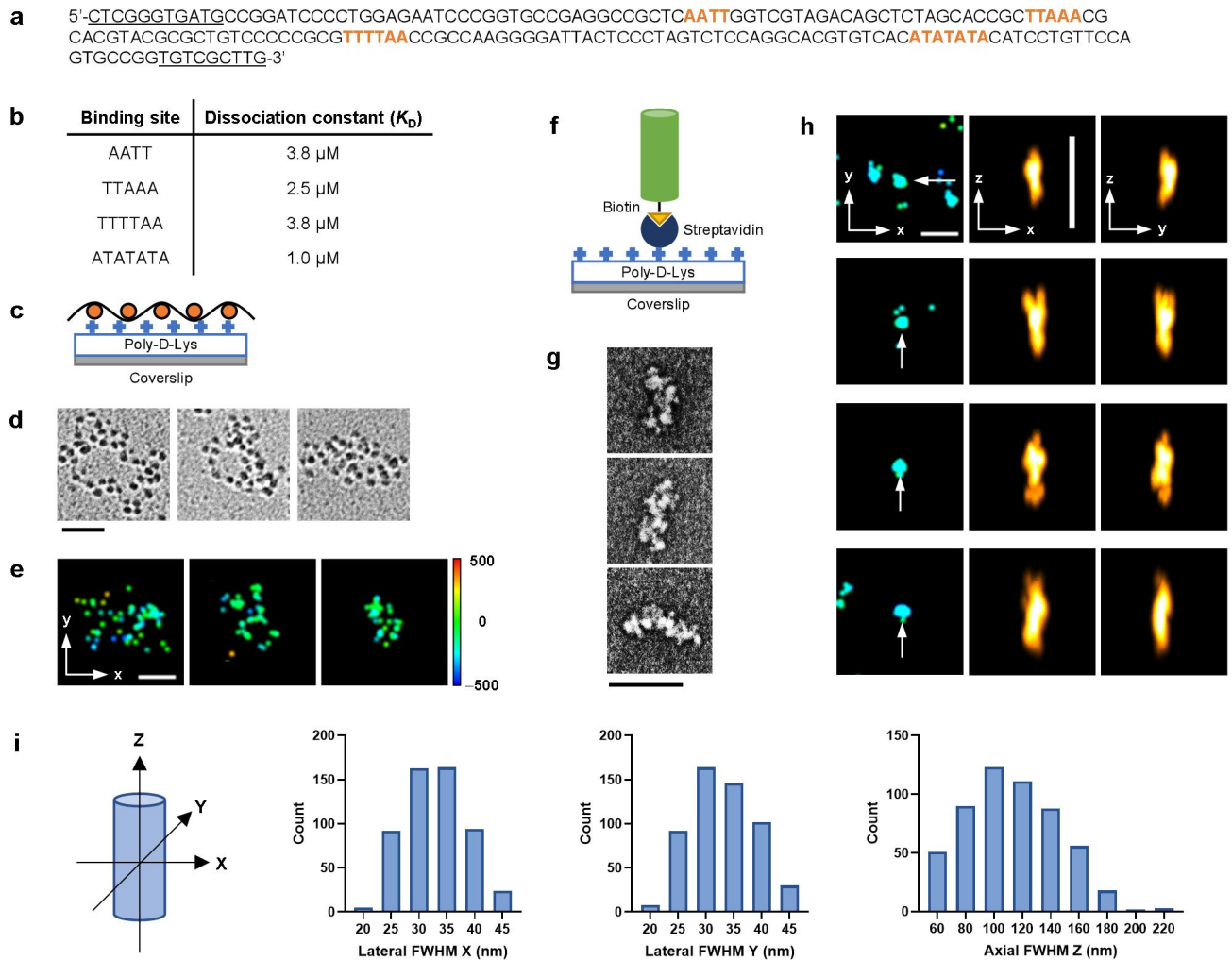
365 for fluorescence titration. **c**, Fluorescence titration of 6-HoeHESiR (0.5  $\mu\text{M}$ ) with hpDNA (0–16  $\mu\text{M}$ )

366 in Tris-HCl saline buffer (50 mM Tris-HCl, 100 mM NaCl, pH = 7.4).  $F_{\text{I,max}}$  at 676 nm. **d**, Fluorescence

367 of 6-HoeHESiR, 6-HESiR and SiR650 (0.5  $\mu\text{M}$ ) in Tris-HCl saline buffer (50 mM Tris-HCl, 100 mM

368 NaCl, pH = 7.4). **e**, Working mechanism of 6-HoeHESiR in the presence of nucleosomes.

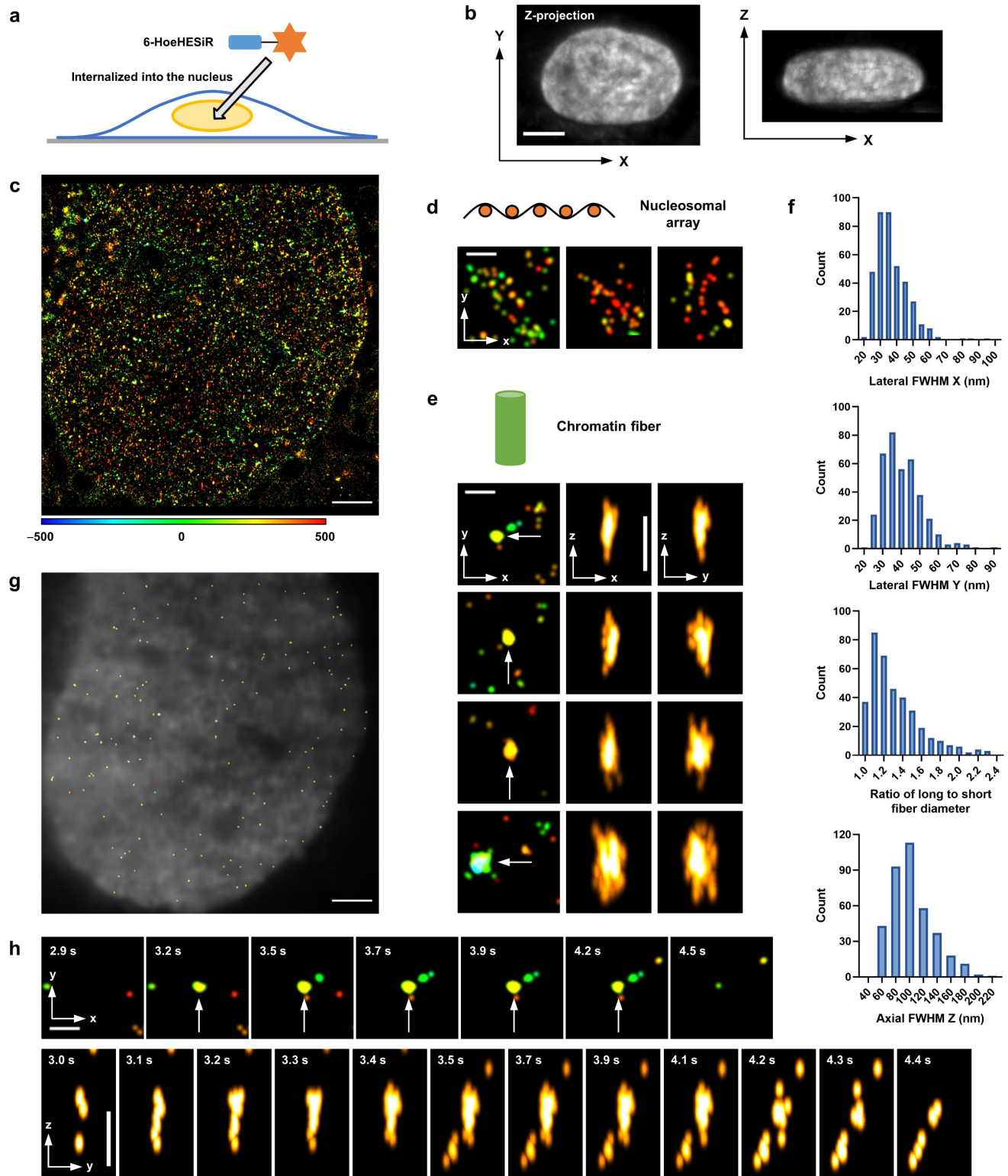
369



370

371 **Fig. 3 *In vitro* reconstituted chromatin structures.** **a**, Sequence of the 187-bp DNA template for  
 372 reconstituted chromatin samples. The linker DNA sequence is underlined. **b**, Summary table of the  
 373 dissociation constants of four binding sites in the DNA template. **c**, Immobilization approach for  
 374 40 $\times$ 187-bp nucleosomal arrays. **d**, EM images of 40 $\times$ 187-bp nucleosomal arrays (metal shadowing). **e**,  
 375 Images of 40 $\times$ 187-bp nucleosomal arrays by 3D SMLM. **f**, Immobilization approach for 40 $\times$ 187-bp  
 376 30-nm chromatin fibers. **g**, EM images of 40 $\times$ 187-bp 30-nm fibers (negative staining). **h**, Images of  
 377 40 $\times$ 187-bp 30-nm fibers by 3D SMLM. FWHM (x, y, z) in nm (from top to bottom.): 27, 29, 81; 27, 29,  
 378 96; 30, 30, 101; 34, 25, 107. Localization precision (nm): 6.3, 6.8, 5.9, 6.7. **i**, 3D sizes of identified  
 379 fibers by FWHM.  $N = 542$  from 3 fields of view. Incubation with **6-HoeHESiR** (2.5  $\mu$ M) for 10 min.

380 Scale bar: 100 nm in **d** and **g**; 200 nm in **e** and **h**. Axial position (nm) represented by RGB color depth  
381 coding.

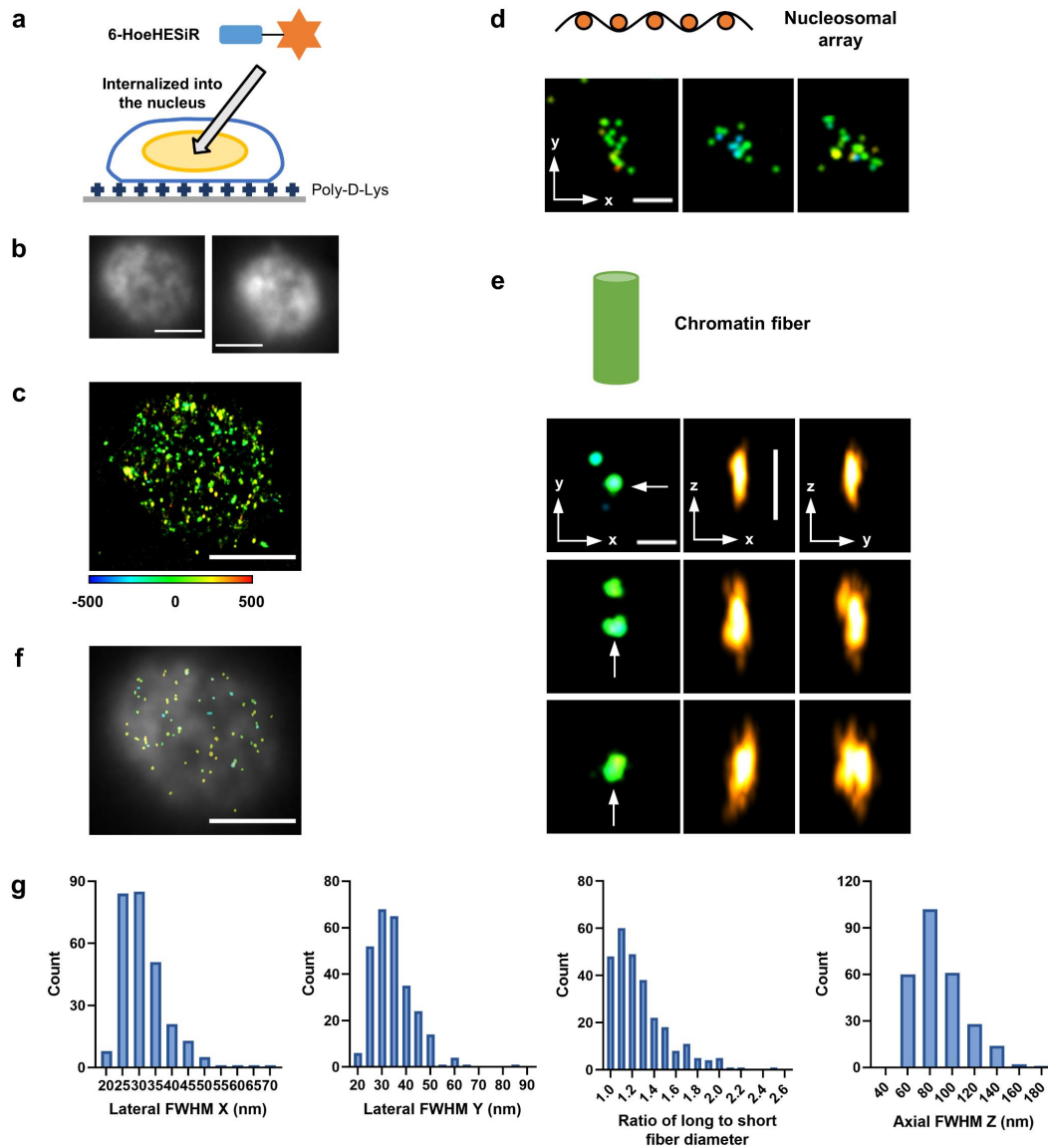


382

383 **Fig. 4 Hierarchical chromatin structures in living HeLa cells.** **a**, Schematic illustration of chromatin  
 384 labeling with 6-HoeHESiR (5  $\mu$ M for 30 min). **b**, Images of a whole nucleus by light-sheet microscopy.  
 385 **c**, Image of a nucleus. Reconstructed with 2,000 frames (17.7 ms/frame). **d**, Nucleosomal arrays. **e**,

386 Chromatin fibers. FWHM (x, y, z) in nm (from top to bottom): 30, 30, 107; 35, 42, 124; 34, 51, 102; 69,  
387 51, 154. Localization precision (nm): 7.6, 6.8, 6.8, 9.5. **f**, 3D sizes of chromatin fibers by FWHM.  $N =$   
388 371 from 3 cells, identified in 500 frames. **g**, Distribution of chromatin fibers (identified in 500 frames).  
389 **h**, Fast dynamics of a chromatin fiber. Snapshots from Supplementary Videos 7 and 8 (Supplementary  
390 Information, video legends). Scale bar: 5  $\mu\text{m}$  in **b**; 2  $\mu\text{m}$  in **c** and **g**; 200 nm in **d**, **e** and **h**. Axial position  
391 (nm) represented by RGB color depth coding.

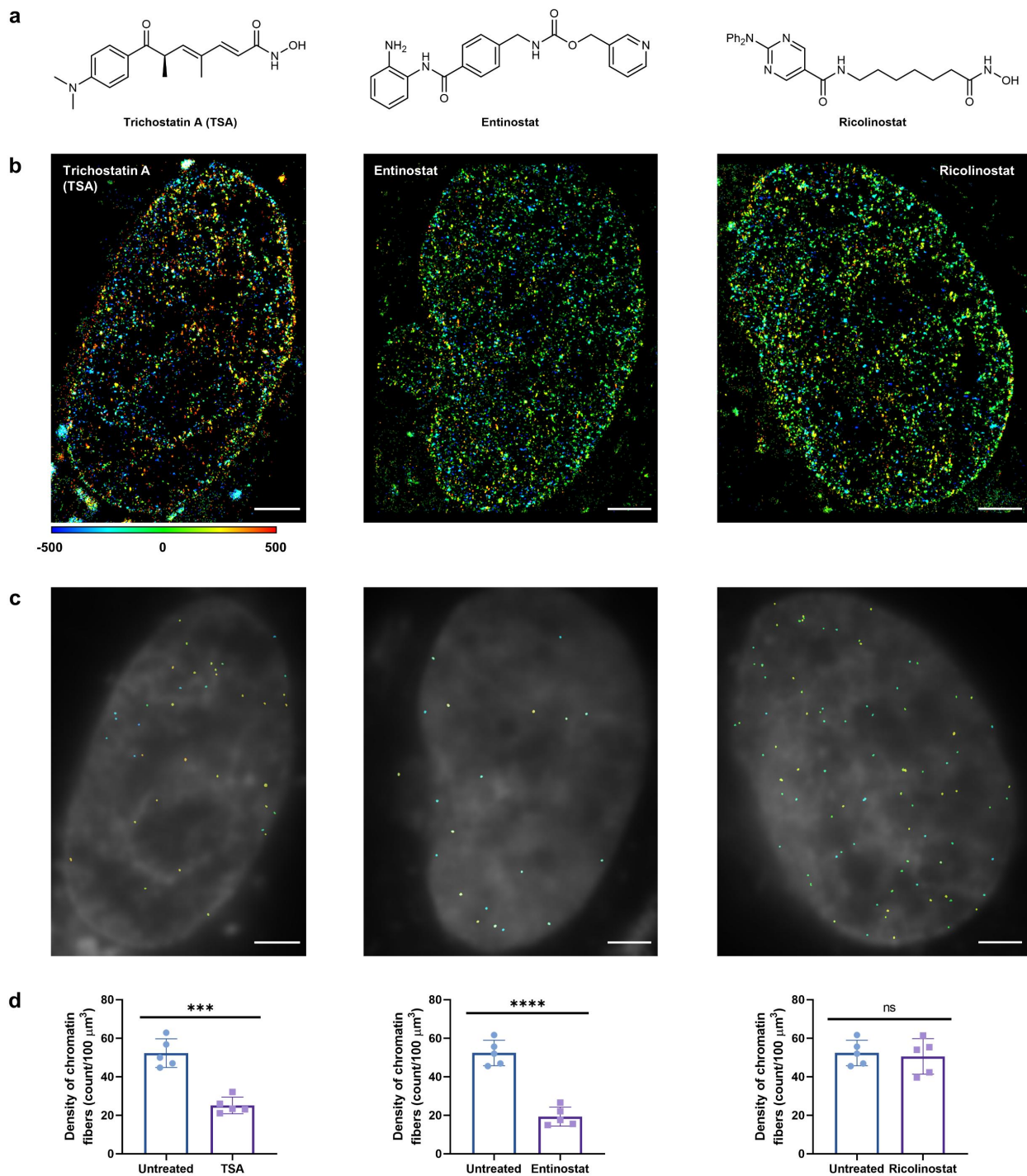
392



393

394 **Fig. 5 Hierarchical chromatin structures in living chicken erythrocytes.** **a**, Schematic illustration of  
 395 chromatin labeling with **6-HoeHESiR** (0.5  $\mu\text{M}$  for 10 min). **b**, Images of two nuclei obtained by  
 396 widefield microscopy. **c**, Image of a nucleus. Reconstructed with 10,000 frames (17.7 ms/frame). **d**,  
 397 Nucleosomal arrays. **e**, Chromatin fibers. FWHM (x, y, z) in nm (from top to bottom): 27, 29, 83; 37, 40,  
 398 124; 40, 62, 95. Localization precision (nm): 6.8, 6.9, 8.1. **f**, 3D sizes of chromatin fibers by FWHM.  $N$   
 399 = 271 from 3 cells, identified in 5,000 frames. **g**, Distribution of chromatin fibers (identified in 5,000  
 400 frames). Scale bar: 2  $\mu\text{m}$  in **b**, **c** and **g**; 200 nm in **d** and **e**. Axial position (nm) represented by RGB  
 401 color depth coding.

402



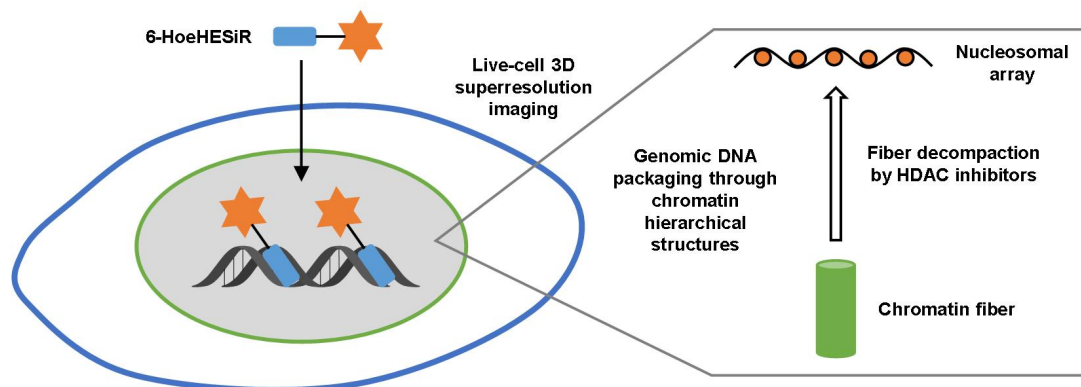
403

404 **Fig. 6 Decompaction of chromatin fibers induced by HDAC inhibitors.** **a**, Structures of  
405 small-molecule inhibitors of HDAC. **b**, Images of the nuclei in treated HeLa cells. Reconstructed with  
406 2,000 frames (17.7 ms/frame). **c**, Distribution of chromatin fibers (identified in 500 frames). **d**, Density  
407 of chromatin fibers (identified in 500 frames). Data are individual values and mean  $\pm$  s.d.,  $N = 5$ .  
408 Statistical significance was determined by *t* test with  $P = 0.0001$ ,  $<0.0001$  and  $0.7278$  (from left to right).

409 The scale bar is 2  $\mu\text{m}$ . Axial position (nm) represented by RGB color depth coding. Cells were treated  
410 with TSA (200 nM), entinostat (2  $\mu\text{M}$ ), and ricolinostat (1  $\mu\text{M}$ ) for 20 h, respectively, and then  
411 incubated with **6-HoeHESiR** (5  $\mu\text{M}$ ) for 30 min.

412

413



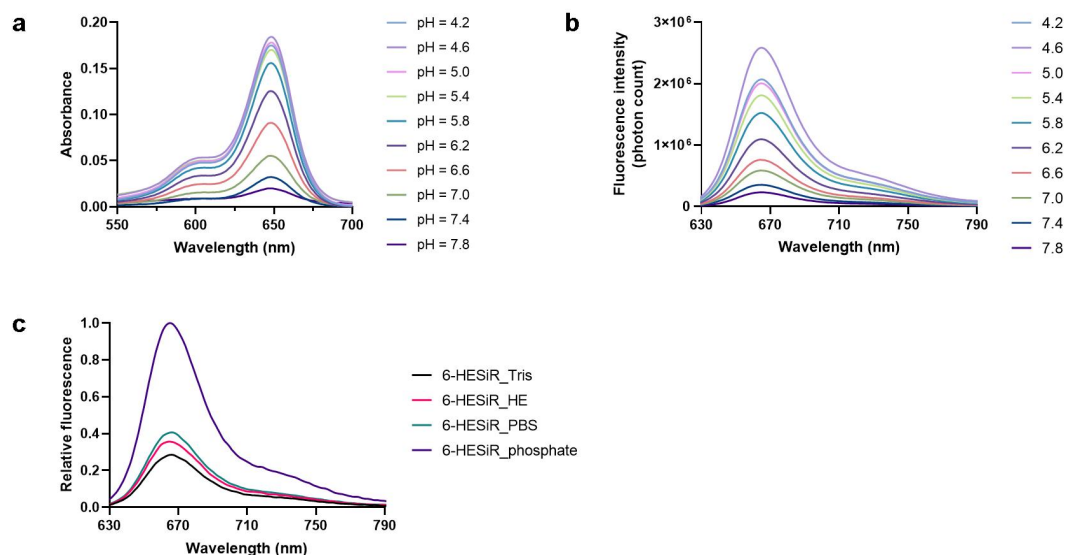
414

415 **Fig. 7** Schematic illustration of genomic DNA packaging via hierarchical chromatin structures in living  
416 cells.

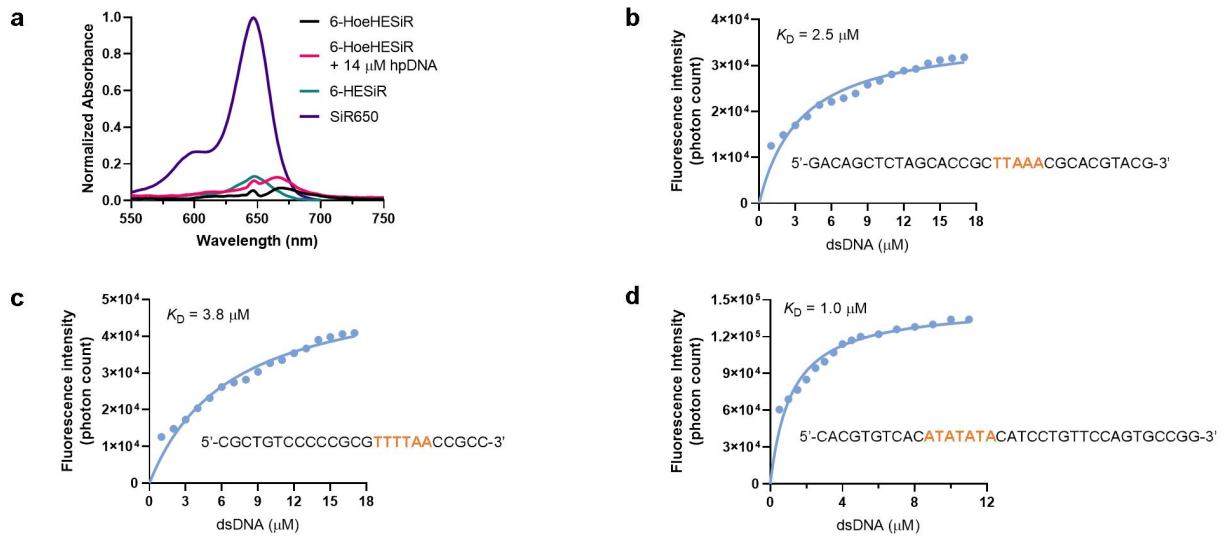


## Supplementary Materials

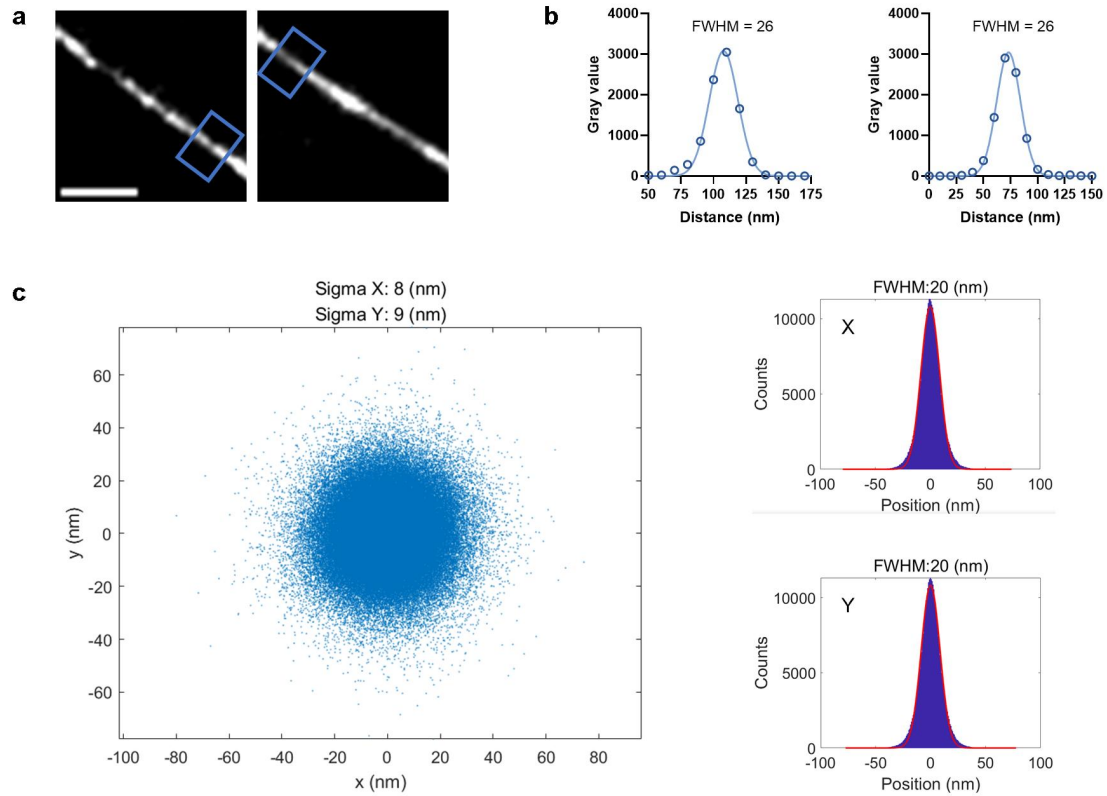
### Supplementary figures



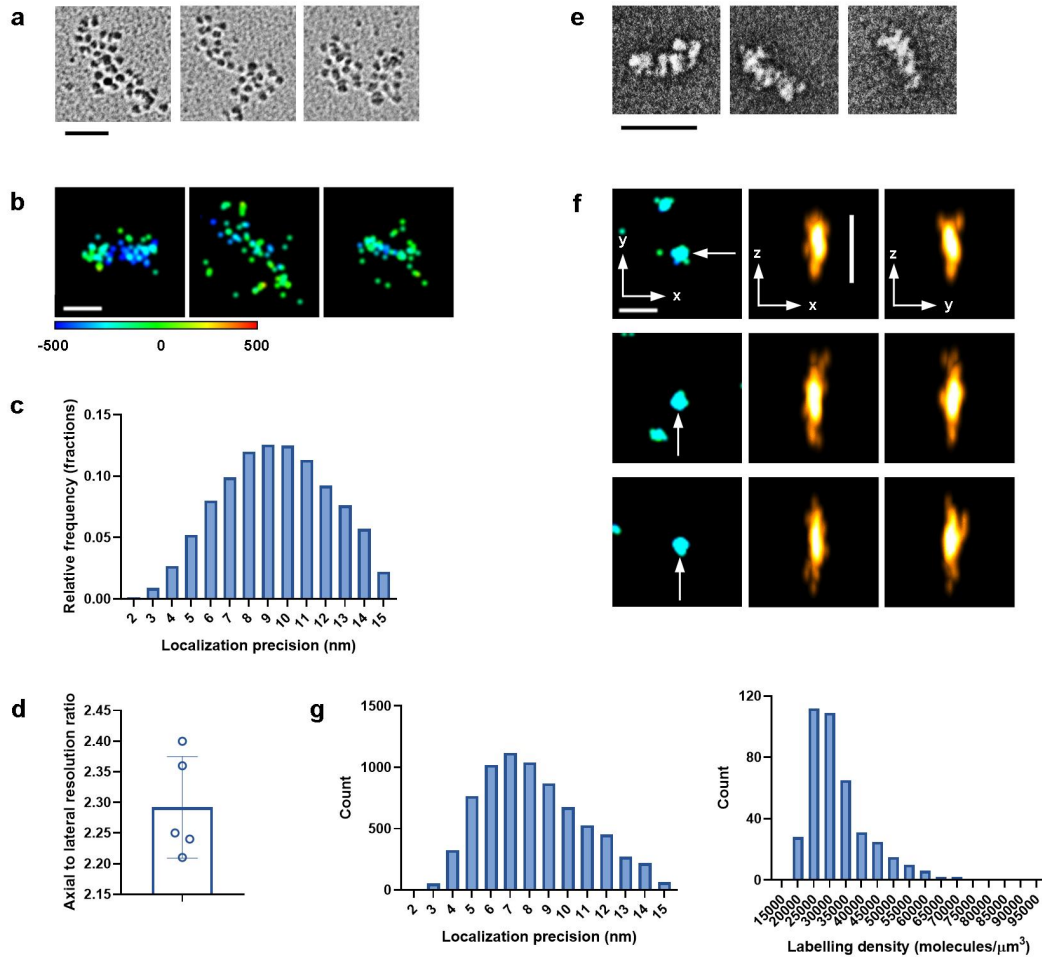
**Supplementary Fig. 1 Photophysical properties of 6-HESiR.** **a**, Absorption spectra of 6-HESiR (2  $\mu\text{M}$ ) at various pH values in 0.1 M potassium phosphate buffer. **b**, Fluorescence emission spectra of 6-HESiR (0.5  $\mu\text{M}$ ) at various pH values in 0.1 M potassium phosphate buffer. **c**, Fluorescence emission spectra of 6-HESiR (2  $\mu\text{M}$ ) in aqueous buffers. Tris: 50 mM Tris-HCl, 100 mM NaCl (pH = 7.4). HE: 10 mM HEPES, 1 mM EDTA (pH = 7.5). PBS: 1  $\times$  (pH = 7.4). Phosphate: 0.1 M potassium phosphate (pH = 7.4).



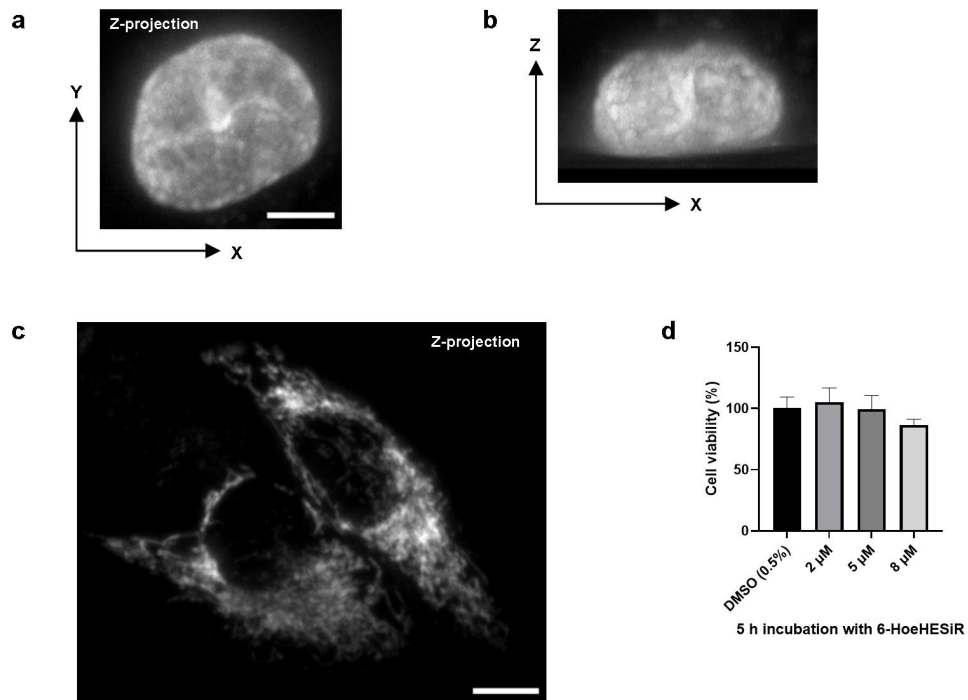
**Supplementary Fig. 2 Fluorescence titration of 6-HoeHESiR.** **a**, Absorbance of 6-HoeHESiR (0.5  $\mu$ M) in Tris-HCl saline buffer.  $Abs_{max}$  at 668 nm. **b-d**, Fluorescence titration with 0.5  $\mu$ M 6-HoeHESiR and dsDNA segments in the Tris-HCl saline buffer.



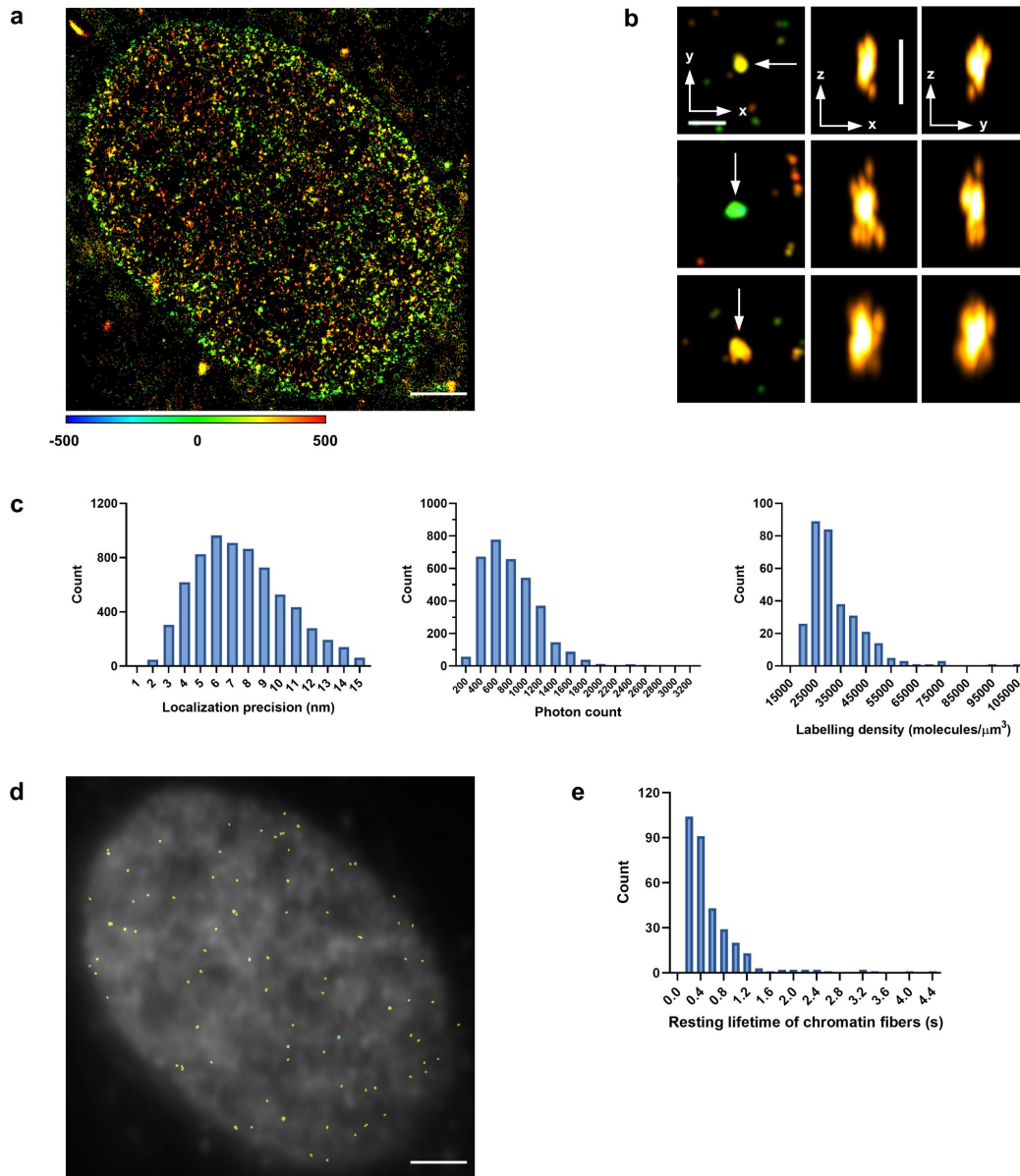
**Supplementary Fig. 3 SMLM with lambda DNA.** **a**, Reconstructed images of spin-coated  $\lambda$ -DNA. **b**, Line profiles for the boxed regions in **a** for obtaining FWHM values. **c**, Localization precision. Imaging performed with 100 nM 6-HoeHESiR. Scale bar: 200 nm.



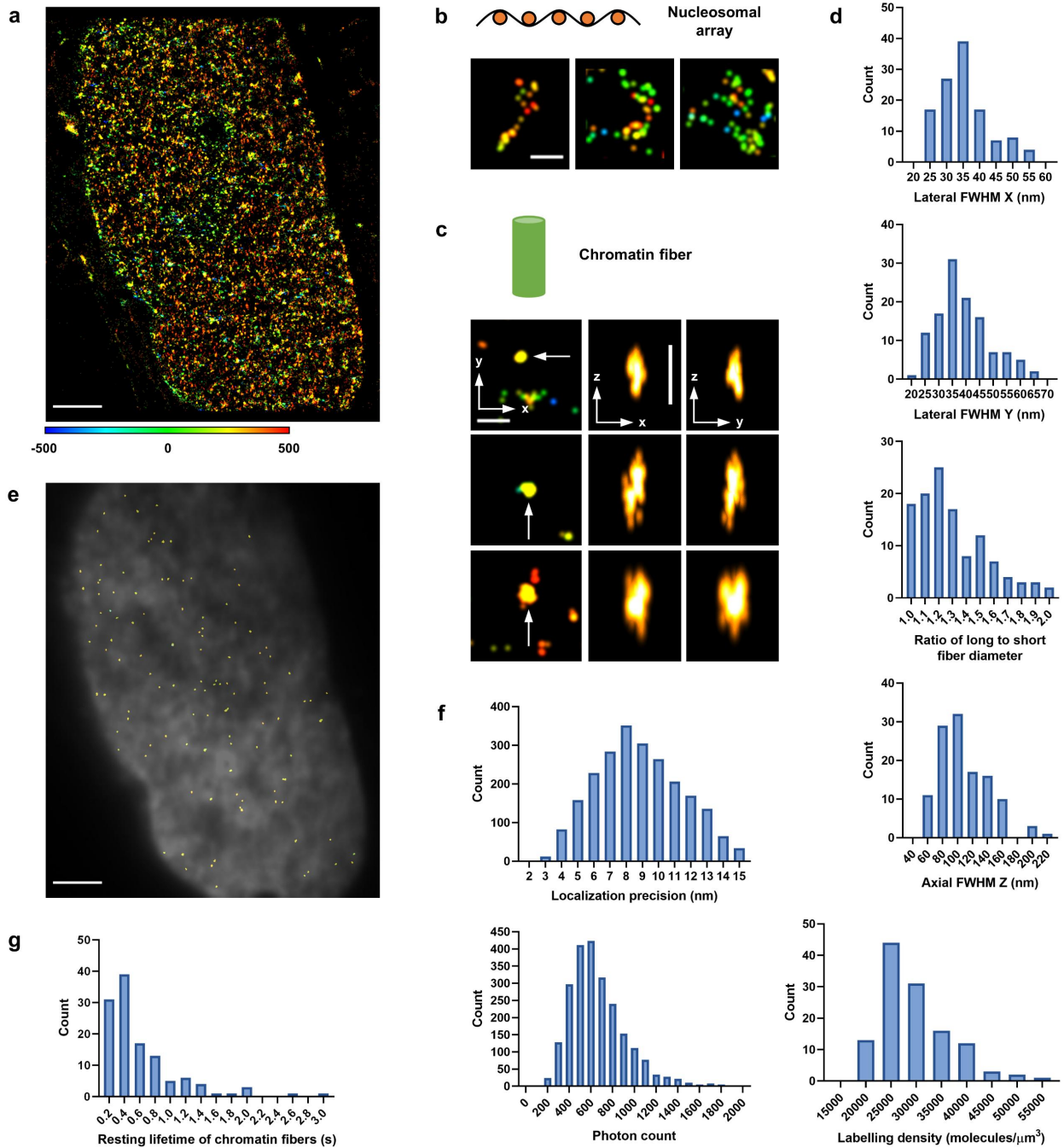
**Supplementary Fig. 4 SMLM with *in vitro* reconstituted chromatin structures.** **a**, EM images of 40×187-bp nucleosomal arrays (by metal-shadowing). **b**, Images of 40×187-bp nucleosomal arrays by 3D SMLM. **c**, Localization precision for 40×187-bp nucleosomal arrays. **d**, Ratio of axial resolution to lateral resolution for individual nucleosomes. Data are mean ± s.d.,  $N = 5$ . **e**, EM images of 40×187-bp 30-nm chromatin fibers (negative staining). **f**, Images of 40×187-bp 30-nm fibers by 3D SMLM. FWHM (x, y, z) in nm: 30, 33, 96; 29, 30, 95; 27, 33, 107. Localization precision (nm): 6.2, 6.7, 6.6. From top to bottom. **g**, Localization precision and labeling density for identified 30-nm chromatin fibers. Incubation with **6-HoeHESiR** (2.5  $\mu\text{M}$ ) for 10 min. Scale bar: 100 nm in **a** and **e**; 200 nm in **b** and **f**. Axial position (nm) represented by RGB color depth coding.



**Supplementary Fig. 5 Light-sheet microscopy of living HeLa cells.** **a**, The Z-projection image of the nucleus in a living HeLa cell. **b**, The XZ projection image of the same nucleus. **c**, The Z-projection image of living HeLa cells stained with **6-HESiR**. **d**, Cytotoxicity assay with **6-HoeHESiR**.  $N = 3$ , data are mean + SD. Incubation with **6-HoeHESiR** (5  $\mu$ M) and **6-HESiR** (2  $\mu$ M) for 30 min, respectively. Scale bar: 5  $\mu$ m in **a** and **b**; 10  $\mu$ m in **c**.



**Supplementary Fig. 6 Chromatin fibers in living HeLa cells.** **a**, The image of a nucleus. Reconstructed from 2,000 frames (17.7 ms/frame). **b**, High-order chromatin fibers. FWHM (x, y, z) in nm (from top to bottom.): 31, 34, 94; 44, 35, 116; 45, 50, 103. Localization precision (nm): 7, 7.2, 9.1. **c**, Localization precision, photon count and labeling density for identified fibers in 500 frames. **d**, The distribution of chromatin fibers (identified in 500 frames). **e**, Lifetime of identified fibers in 500 frames. Incubation with 6-HoeHESiR (5  $\mu$ M) for 30 min. Scale bar: 2  $\mu$ m in **a** and **d**; 200 nm in **b**. Axial position (nm) represented by RGB color depth coding.



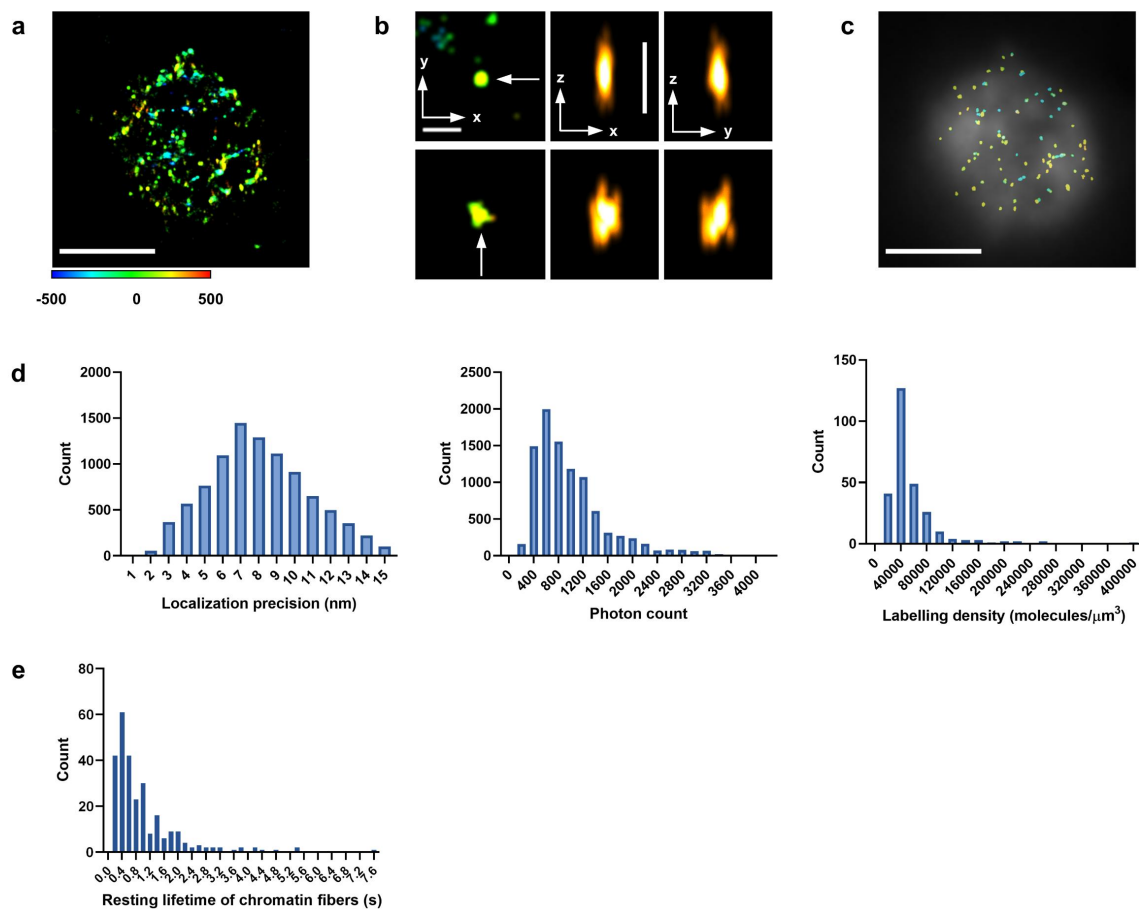
**Supplementary Fig. 7 Hierarchical chromatin structures in a living HeLa cell with reduced phototoxicity. a**, The image of a nucleus. Reconstructed from 2,000 frames (17.7 ms/frame). **b**, Images of nucleosomal arrays. **c**, Chromatin fibers. FWHM (x, y, z) in nm (from top to bottom): 31, 33, 95; 42, 36, 130; 47, 62, 112. Localization precision (nm): 6.8, 7.2, 8.9. **d**, 3D sizes of identified fibers in 500 frames.  $N = 119$ . **e**, The distribution of chromatin fibers (identified in 500 frames). **f**,

Localization precision, photon count and labeling density for identified fibers in 500 frames. **g**,

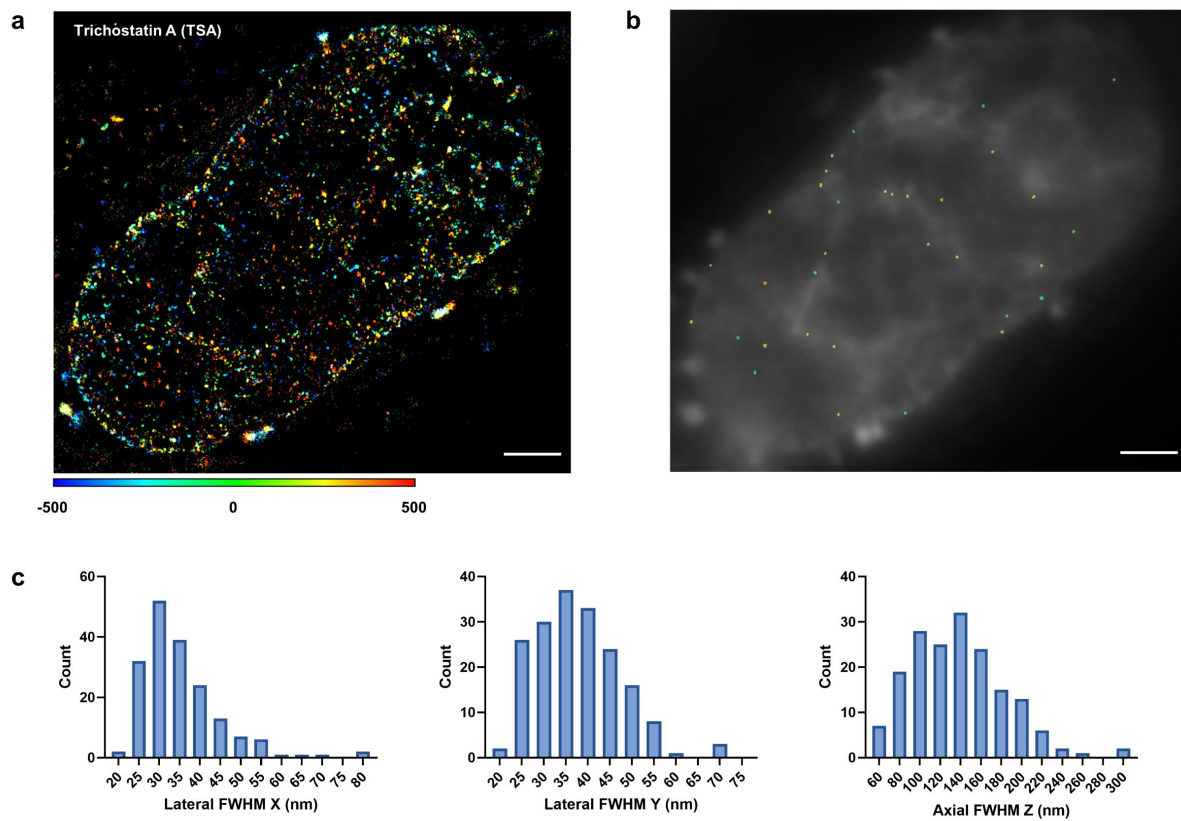
Lifetime of identified fibers in 500 frames. Incubation with **6-HoeHESiR** (5  $\mu$ M) for 30 min. Scale

bar: 2  $\mu$ m in **a** and **e**; 200 nm in **b** and **c**. Axial position (nm) represented by RGB color depth coding.

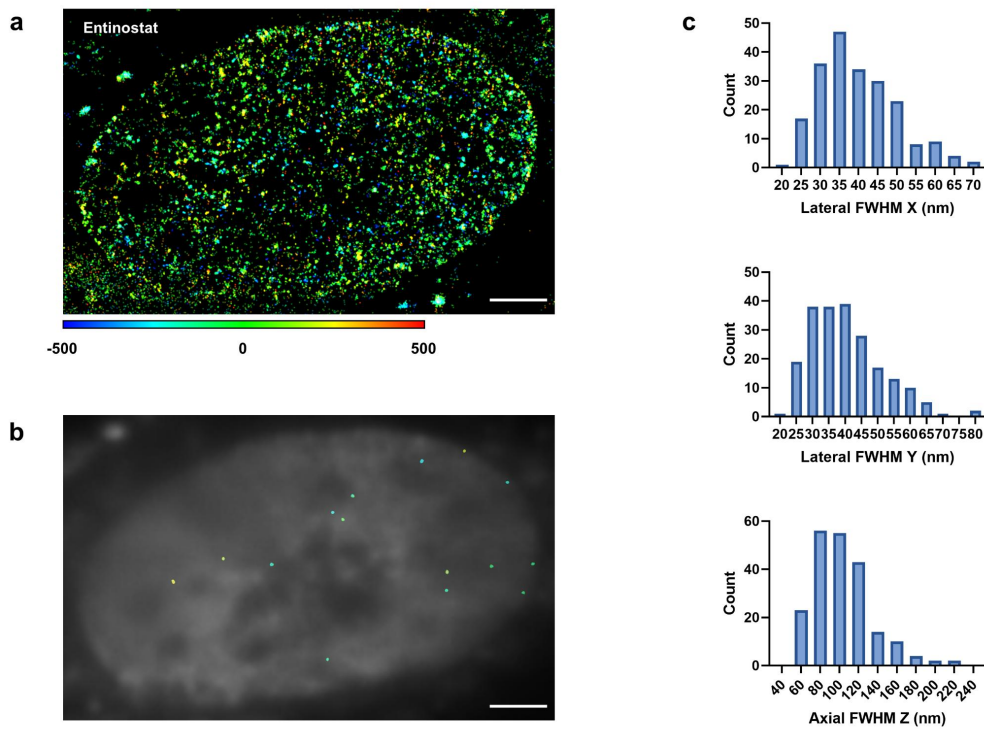




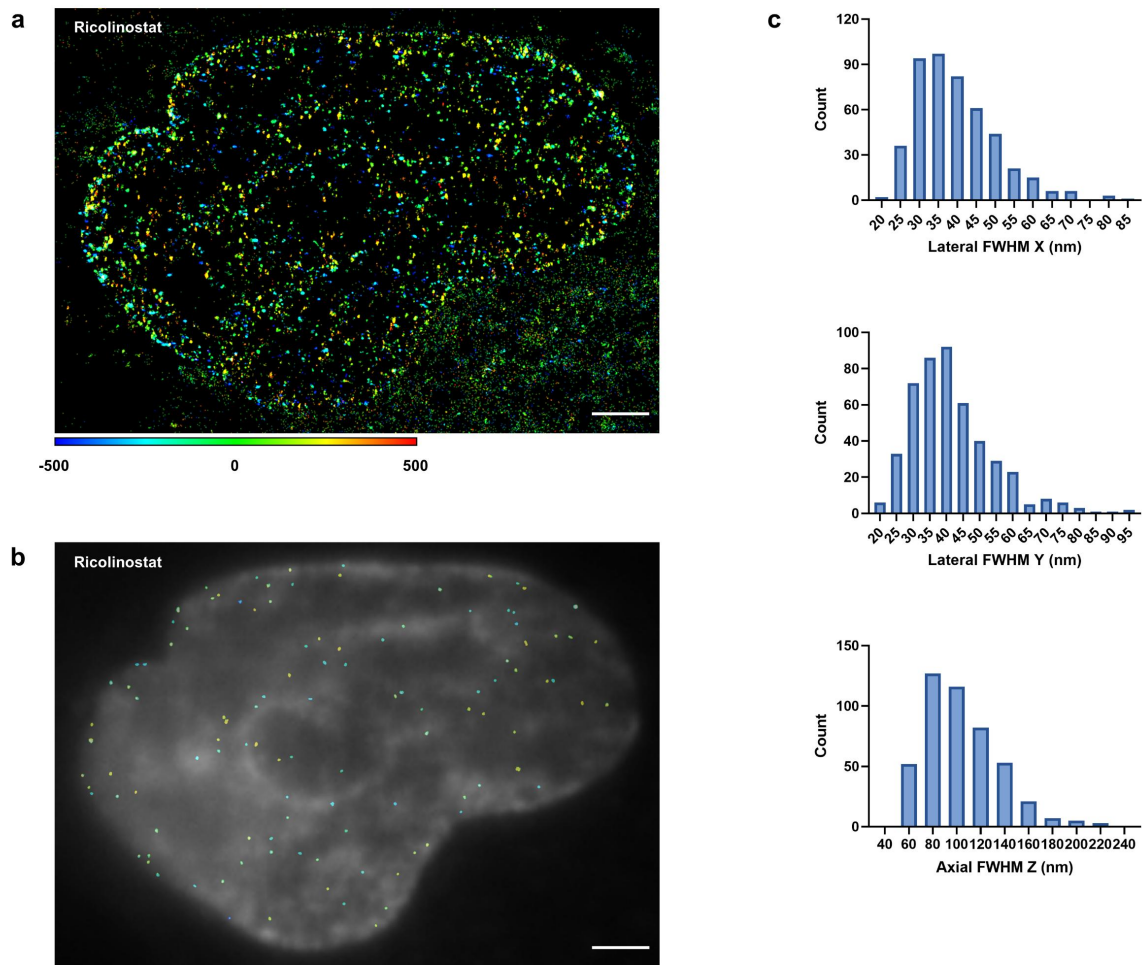
**Supplementary Fig. 8 High-order chromatin fibers in living chicken erythrocytes.** **a**, The image of a nucleus. Reconstructed with 5,000 frames (17.7 ms/frame). **b**, Chromatin fibers. FWHM (x, y, z) in nm (upper, lower): 25, 33, 84; 51, 47, 94. Localization precision (nm): 7.4, 8.5. **c**, The distribution of chromatin fibers (data from 5,000 frames). **d**, Localization precision, photon count and labeling density for identified fibers in 5,000 frames. **e**, Lifetime of identified fibers in 5,000 frames. Incubation with **6-HoeHESiR** (0.5 μM) for 10 min. Scale bar: 2 μm in **a** and **c**; 200 nm in **b**. Axial position (nm) represented by RGB color depth coding.



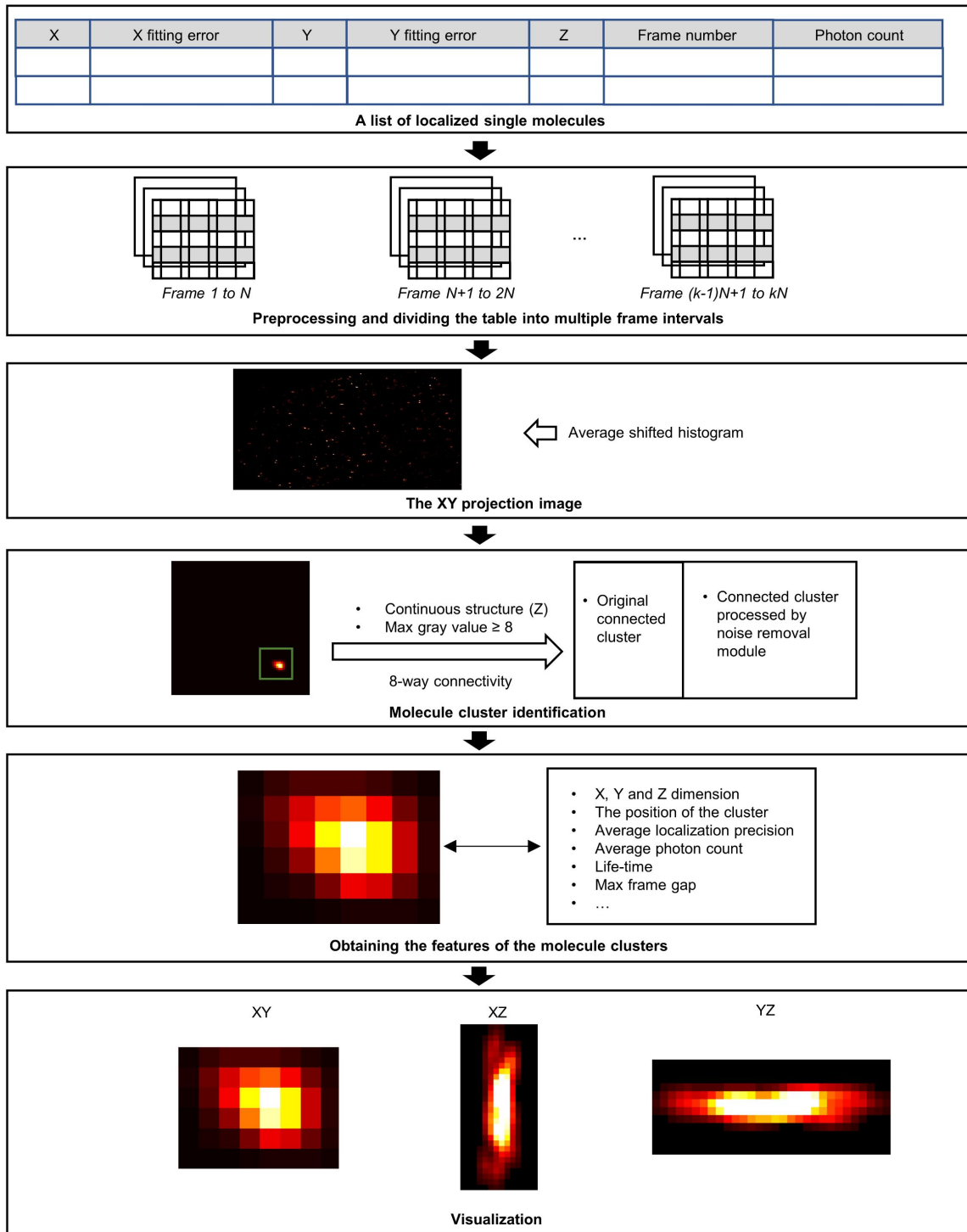
**Supplementary Fig. 9 Treatment with trichostatin A.** **a**, The nucleus of a treated HeLa cell. Reconstructed with 2,000 frames (17.7 ms/frame). **b**, The distribution of chromatin fibers (identified in 500 frames). **c**, 3D sizes of chromatin fibers from 5 cells.  $N = 180$ . Identified in 500 frames. Incubation with **6-HoeHESiR** (5  $\mu\text{M}$ ) for 30 min. Scale bar is 2  $\mu\text{m}$ . Axial position (nm) represented by RGB color depth coding.



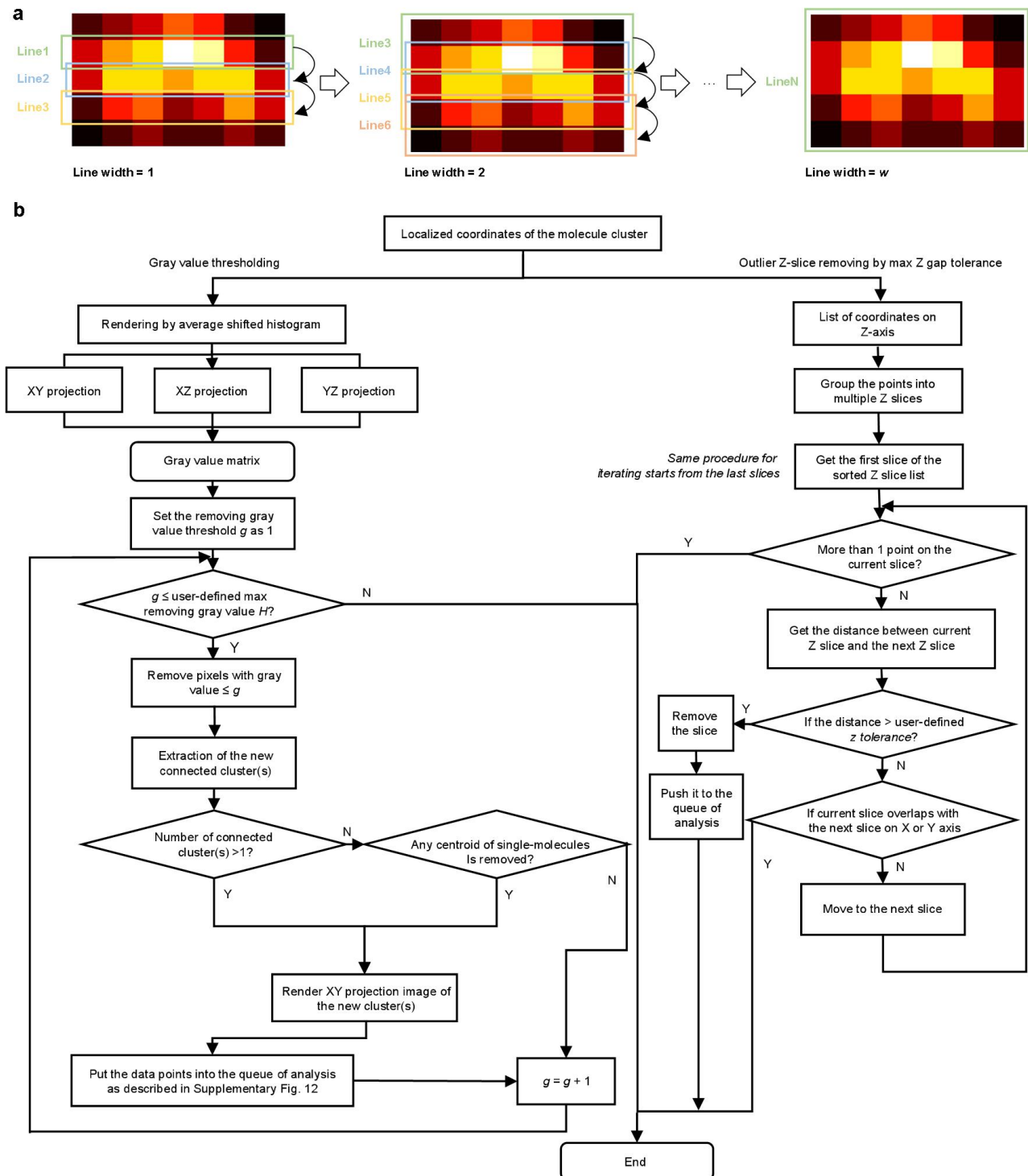
**Supplementary Fig. 10 Treatment with entinostat.** **a**, The nucleus of a treated HeLa cell. Reconstructed with 2,000 frames (17.7 ms/frame). **b**, The distribution of chromatin fibers (identified in 500 frames). **c**, 3D sizes of chromatin fibers from 5 cells.  $N = 211$ . Identified in 500 frames. Incubation with **6-HoeHESiR** (5  $\mu$ M) for 30 min. Scale bar is 2  $\mu$ m. Axial position (nm) represented by RGB color depth coding.



**Supplementary Fig. 11 Treatment with ricolinostat.** **a**, The nucleus of a treated HeLa cell. Reconstructed with 2,000 frames (17.7 ms/frame). **b**, The distribution of chromatin fibers (identified in 500 frames). **c**, 3D sizes of chromatin fibers from 5 cells.  $N = 468$ . Identified in 500 frames. Incubation with **6-HoeHESiR** (5  $\mu\text{M}$ ) for 30 min. Scale bar is 2  $\mu\text{m}$ . Axial position (nm) represented by RGB color depth coding.



**Supplementary Fig. 12** The flowchart of the analysis of molecular clusters for identification of chromatin fibers.



**Supplementary Fig. 13 Chromatin fiber analysis program. a**, The demonstration of the moving line strategy for estimating X dimension of molecular clusters. **b**, The flowchart of the noise removal module, which consists of two submodules: gray value thresholding and outlier Z slice removing by max Z gap tolerance.  $g$  ranges from 1 to the user-defined max threshold  $H$ .

## Supplementary video legends

1. Self-blinking of **6-HoeHESiR** in a 3D SMLM experiment of *in vitro* reconstituted 30-nm chromatin fibers. Scale bar: 2  $\mu\text{m}$ . 950  $\text{W}/\text{cm}^2$  laser intensity at 656 nm. Camera exposure at 17.7 ms/frame.
2. 3D rotation of an *in vitro* reconstituted chromatin fiber in Fig. 3h. Scale bar: 200 nm.
3. 3D rotation of another *in vitro* reconstituted chromatin fiber in Fig. 3h. Scale bar: 200 nm.
4. Self-blinking of **6-HoeHESiR** in a 3D SMLM experiment of a living HeLa cell. Scale bar: 2  $\mu\text{m}$ . 3.2  $\text{kW}/\text{cm}^2$  laser intensity at 656 nm. Camera exposure at 17.7 ms/frame.
5. 3D rotation of a chromatin fiber in a HeLa cell in Fig. 4e.
6. 3D rotation of another chromatin fiber in a HeLa cell in Fig. 4e.
7. Time-lapse video (z-projection) of dynamic chromatin structures in a living HeLa cell. 56 frames per image. 5 frames per sliding window. Scale bar: 2  $\mu\text{m}$ . 3.2  $\text{kW}/\text{cm}^2$  laser intensity at 656 nm. Camera exposure at 17.7 ms/frame. Axial position is represented by RGB color depth coding.
8. Time-lapse video (yz-projection) of a chromatin fiber in Fig. 4e. 56 frames per image. 5 frames per sliding window. Scale bar: 200 nm. 3.2  $\text{kW}/\text{cm}^2$  laser intensity at 656 nm. Camera exposure at 17.7 ms/frame.
9. Time-lapse video (z-projection) of chromatin dynamics in a living HeLa cell with reduced phototoxicity. 56 frames per image. 5 frames per sliding window. Scale bar: 2  $\mu\text{m}$ . 950  $\text{W}/\text{cm}^2$  laser intensity at 656 nm. Camera exposure at 17.7 ms/frame. Axial position is represented by RGB color depth coding.
10. Self-blinking of **6-HoeHESiR** in a 3D SMLM experiment of a living chicken erythrocyte. Scale bar: 2  $\mu\text{m}$ . 950  $\text{W}/\text{cm}^2$  laser intensity at 656 nm. Camera exposure at 17.7 ms/frame.
11. 3D rotation of a chromatin fiber in a chicken erythrocyte in Fig. 5e. Scale bar: 200 nm.
12. 3D rotation of another chromatin fiber of a chicken erythrocyte in Fig. 5e. Scale bar: 200 nm.

13. Time-lapse video (z-projection) of chromatin dynamics in a living chicken erythrocyte with reduced phototoxicity. 56 frames per image. 5 frames per sliding window. Scale bar: 2  $\mu\text{m}$ . 950  $\text{W}/\text{cm}^2$  laser intensity at 656 nm. Camera exposure at 17.7 ms/frame. Axial position is represented by RGB color depth coding.

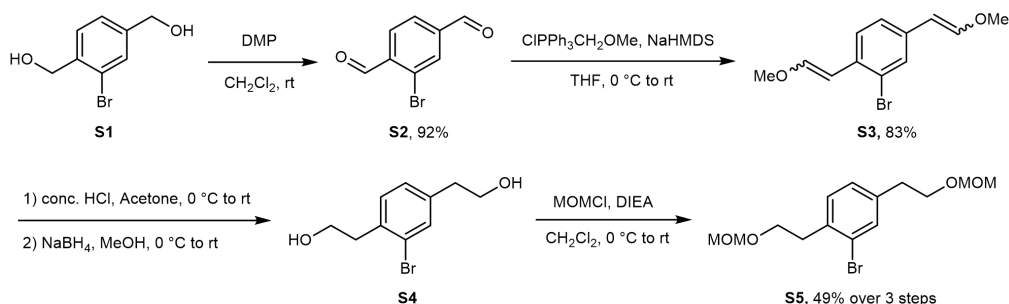


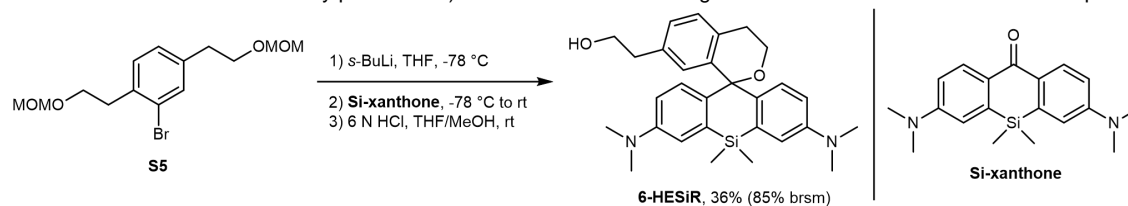
## Chemical synthesis and characterization

### General information

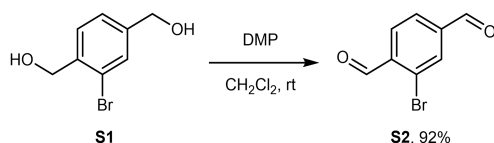
NMR spectra were acquired on Bruker 400 and 500 MHz spectrometers. High resolution mass spectra were acquired on Bruker maXis II and Thermo Scientific DFS. Preparative reverse phase HPLC was performed on a Waters preparative HPLC system with a C18 reverse phase column. All chemicals and reagents were purchased from commercial sources and used without further purification. Dess-Martin periodinane (DMP), dry *N,N*-diisopropylethylamine (DIEA), triethylamine and trifluoroacetic acid (TFA) were purchased from Energy Chemical. DIEA was purchased from TCI.  $\text{ClPh}_3\text{PCH}_2\text{OMe}$  and Hoechst 33258 were purchased from J&K. NaHMDS was purchased from Alfa Aesar.  $\text{NaBH}_4$  was purchased from Lancaster Synthesis. Chloromethyl methyl ether (MOMCl) was purchased from Sigma Aldrich. *s*-BuLi was purchased from Infinity Scientific. 4-Nitrophenyl chloroformate was purchased from Apollo Scientific. All solvents were either AR or HPLC grade. Dry dichloromethane ( $\text{CH}_2\text{Cl}_2$ ) and dry tetrahydrofuran (THF) were obtained from a solvent purification system. Dry dimethylformamide (DMF) was purchased from Energy Chemical. Deuterated solvents  $\text{CDCl}_3$  and  $\text{CD}_3\text{OD}$  for NMR experiments were purchased from Cambridge Isotope Laboratories.

### Synthetic route of 6-HESiR

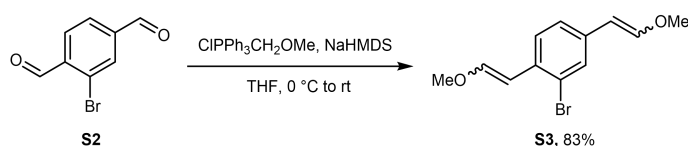




## Procedures for making 6-HESiR

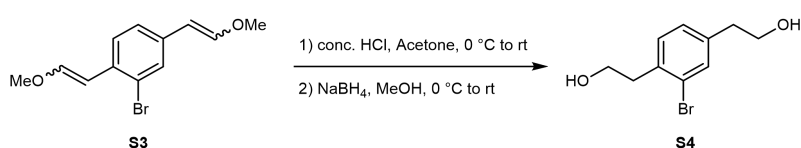


**S1**<sup>1</sup> (0.868 g, 4 mmol) and Dess-Martin periodinane (3.64 g, 8.4 mmol) were added to a 100 mL round-bottom flask, followed by CH<sub>2</sub>Cl<sub>2</sub> (40 mL). The mixture was stirred at room temperature for 3 h. The milky suspension was quenched by saturated NaHCO<sub>3</sub> and extracted with CH<sub>2</sub>Cl<sub>2</sub> three times. The combined organic phase was dried over MgSO<sub>4</sub>, filtered and concentrated. The crude product was purified by flash column chromatography (10% to 20% ethyl acetate/hexane) to give the known compound **S2**<sup>2</sup> as a white solid (0.788 g, 3.7 mmol, 92% yield).

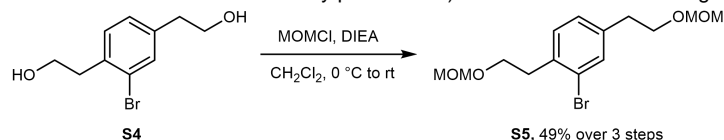


To a 100 mL round-bottom flask with ClPPh<sub>3</sub>PCH<sub>2</sub>OMe (1.58 g, 4.49 mmol, dried before reaction) under argon (Ar) was added THF (anhydrous, 7 mL). The flask was cooled in an ice/water bath with stirring under Ar. 2 M THF solution of NaHMDS (2.25 mL, 4.5 mmol) was added at 0 °C and the resulting mixture was stirred at the same temperature for 1 h. **S2** (0.318 g, 1.49 mmol) dissolved in THF (anhydrous, 4 mL) was transferred to the first flask. Bath was removed and the reaction mixture was warmed to rt and stirred overnight. On the next day, the reaction was quenched with sat. NH<sub>4</sub>Cl, diluted with ethyl acetate (EA) and water, and extracted with EA three times. The combined organic phase was dried over MgSO<sub>4</sub>, filtered and concentrated. The crude product was purified by flash

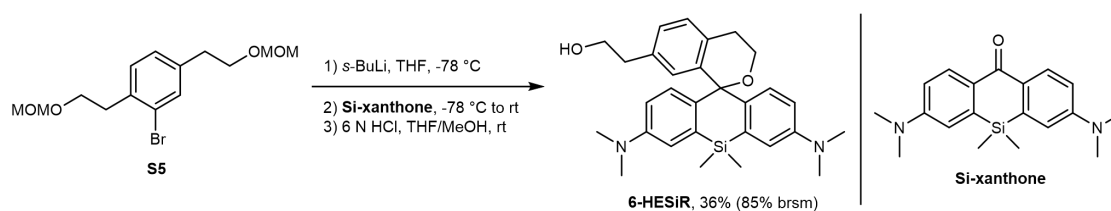
column chromatography (15% CH<sub>2</sub>Cl<sub>2</sub>/hexane, then 5% EA/hexane) to give **S3** as a light-yellow oil (0.332 g, 1.23 mmol, 83% yield). Due to instability of **S3**, only <sup>1</sup>H NMR spectrum was acquired. Due to complexity of the spectrum caused by two pairs of E/Z isomers, only integral ratios are provided. <sup>1</sup>H NMR (500 MHz, CDCl<sub>3</sub>) δ 7.97–7.93, 7.81–7.78, 7.41–7.36, 7.25–7.22, 7.11–7.06 (3H, aromatic protons), 7.04–6.95, 6.22–6.20, 6.14–6.12, 6.09–6.04, 5.72–5.69, 5.59–5.56, 5.13–5.11 (4H, vinylic protons), 3.79–3.77, 3.72, 3.68 (6H, protons of two methyl groups).



**S3** (0.332 g, 1.23 mmol) was dissolved with acetone (13 mL) in a 100 mL round-bottom flask and the solution was cooled in an ice/water bath. Concentrated HCl (1 mL) was added to the solution and the mixture was stirred for 30 min at 0 °C. Then bath was removed, and the reaction was warmed to room temperature and stirred for another 1.5 h. The reaction was quenched with sat. NaHCO<sub>3</sub> and extracted three times with EA. The combined organic phase was washed with brine, dried over MgSO<sub>4</sub>, filtered, and concentrated. Then methanol (14 mL) was added, and the round-bottom flask was cooled in an ice/water bath with stirring. NaBH<sub>4</sub> (0.375 g, 12.3 mmol) was added carefully (gas evolution) at 0 °C. The reaction mixture was stirred at the same temperature for 30 min. Then bath was removed, and the reaction was warmed to room temperature and stirred overnight (reaction time unoptimized). On the next day, saturated NaHCO<sub>3</sub> was added and EA was used to extract the mixture three times. The combined organic phase was washed with brine, dried over MgSO<sub>4</sub>, filtered, and concentrated. The crude product was purified by flash column chromatography (2% to 4% MeOH/CH<sub>2</sub>Cl<sub>2</sub>) to give **S4** as a light-yellow viscous oil mixed with inseparable impurities, which was used for the next step without further purification. The crude product could also be directly used for the next step without flash column chromatography.



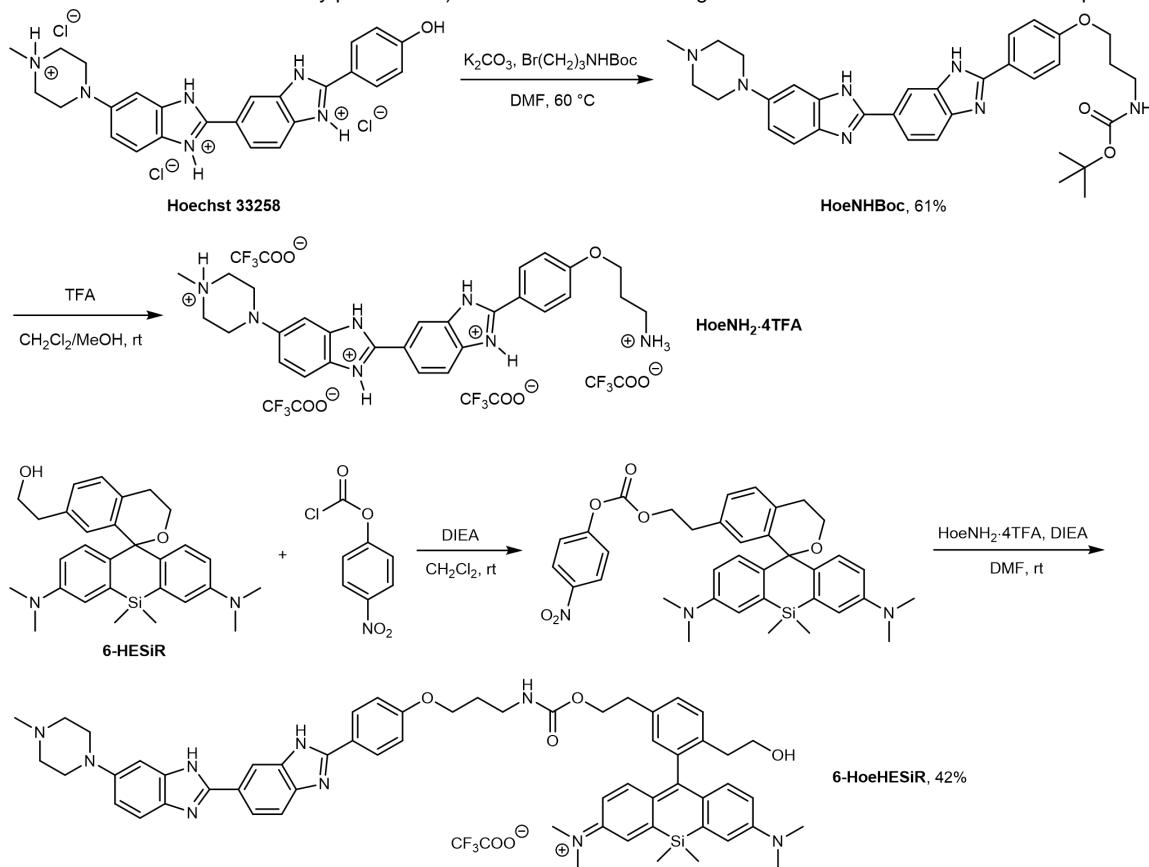
To a 100 mL round-bottom flask with **S4** under Ar were added dry  $\text{CH}_2\text{Cl}_2$  (12 mL) and dry DIEA (1.26 mL, 7.38 mmol) sequentially. The flask was cooled in an ice/water bath with stirring under Ar. MOMCl (0.52 mL, 6.15 mmol) was added dropwise at 0 °C. The reaction mixture was gradually warmed to room temperature and stirred overnight (reaction time unoptimized). On the next day, the reaction was quenched with water and extracted three times with  $\text{CH}_2\text{Cl}_2$ . The combined organic phase was dried over  $\text{MgSO}_4$ , filtered and concentrated. The crude product was purified by flash column chromatography (5% to 10% EA/hexane) to give **S5** as a colorless oil (200 mg, 0.6 mmol, 49% yield over 3 steps).  $^1\text{H}$  NMR (500 MHz,  $\text{CDCl}_3$ )  $\delta$  7.44 (d,  $J = 1.4$  Hz, 1H), 7.20 (d,  $J = 7.8$  Hz, 1H), 7.11 (dd,  $J = 7.8, 1.4$  Hz, 1H), 4.62 (s, 2H), 4.61 (s, 2H), 3.75 (t,  $J = 7.5$  Hz, 2H), 3.74 (t,  $J = 7.3$  Hz, 2H), 3.31 (s, 3H), 3.30 (s, 3H), 3.02 (t,  $J = 7.1$  Hz, 2H), 2.85 (t,  $J = 6.8$  Hz, 2H);  $^{13}\text{C}$  NMR (100 MHz,  $\text{CDCl}_3$ )  $\delta$  139.5, 136.1, 133.4, 131.2, 128.3, 124.8, 96.7, 96.6, 68.3, 67.0, 55.54, 55.48, 36.4, 35.7; HRMS (EI): calcd for  $\text{C}_{14}\text{H}_{21}\text{BrO}_4$  ( $\text{M}^+$ ): 332.0623, 334.0603, found: 332.0613, 334.0600.



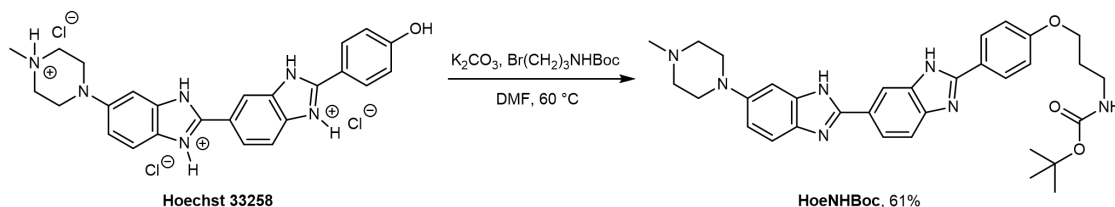
To a 100 mL round-bottom flask with **S5** (0.31 g, 0.93 mmol) under Ar was added THF (anhydrous, 4 mL). The solution was cooled in a dry ice/acetone bath with stirring. *s*-BuLi solution (0.97 mL, 0.96 M in hexane) was added dropwise at  $-78^\circ\text{C}$  and the resulting mixture was stirred for 3.5 h at the same temperature under Ar. Si-xanthone<sup>3</sup> (0.32 g, 0.99 mmol) was suspended in dry THF (sonication applied) and transferred to the first flask under Ar. This suspension/transfer operation was repeated several times (11 mL anhydrous THF in total) and THF (anhydrous, 2 mL) was added

at the end to rinse the remaining residue. Upon completed transfer of Si-xanthone, the cold bath was removed, and the reaction was warmed to room temperature and stirred overnight (reaction time unoptimized). The flask was wrapped with aluminum foil to shield it from light. On the next day, the reaction was quenched with saturated  $\text{NH}_4\text{Cl}$  and a small amount of 1 N HCl. The resulting deep blue mixture was diluted with water and extracted four times with  $\text{CH}_2\text{Cl}_2$ . The combined organic phase was dried over  $\text{Na}_2\text{SO}_4$ , filtered and concentrated. Then THF (4 mL) and MeOH (4 mL) were added, followed by 6 N HCl (10 mL). The reaction mixture was stirred at room temperature overnight (reaction time unoptimized). On the next day, the reaction mixture was diluted with water and quenched with solid  $\text{Na}_2\text{CO}_3$  carefully (gas evolution). EA was added and the mixture was stirred vigorously until the deep blue color faded. Then the mixture was extracted with EA four times. The combined organic phase was washed with brine, dried over  $\text{MgSO}_4$ , filtered, and concentrated. The crude product was purified by flash column chromatography (20% EA/20%  $\text{CH}_2\text{Cl}_2$ /1% triethylamine/hexane to 50% EA/20%  $\text{CH}_2\text{Cl}_2$ /1% triethylamine/hexane) to give **6-HESiR** as a light blue foam (160 mg, 0.338 mmol, 36% yield). Based on recovered Si-xanthone (190 mg), the yield of **6-HESiR** based on recovered starting material (brsm) was 85%.  $^1\text{H}$  NMR (500 MHz,  $\text{CDCl}_3$ )  $\delta$  7.18 (d,  $J = 7.8$  Hz, 1H), 7.14 (d,  $J = 7.8$  Hz, 1H), 7.06 (s, 2H), 6.89 (s, 1H), 6.72 (d,  $J = 8.8$  Hz, 2H), 6.50 (d,  $J = 8.7$  Hz, 2H), 3.76 (t,  $J = 6.6$  Hz, 2H), 3.58 (t,  $J = 5.2$  Hz, 2H), 2.93 (s, 12H), 2.81 (t,  $J = 5.2$  Hz, 2H), 2.76 (t,  $J = 6.5$  Hz, 2H), 0.62 (s, 3H), 0.49 (s, 3H);  $^{13}\text{C}$  NMR (125 MHz,  $\text{CDCl}_3$ )  $\delta$  148.8, 139.3, 139.0, 138.3, 134.7, 134.6, 131.4, 130.5, 129.1, 127.3, 117.7, 112.1, 82.2, 63.9, 59.2, 40.6, 39.0, 29.2, 1.2, -2.7; HRMS (ESI): calcd for  $\text{C}_{29}\text{H}_{36}\text{N}_2\text{O}_2\text{Si}$  ( $[\text{M} + \text{H}]^+$ ): 473.2619, found: 473.2622.

### Synthetic route of 6-HoeHESiR

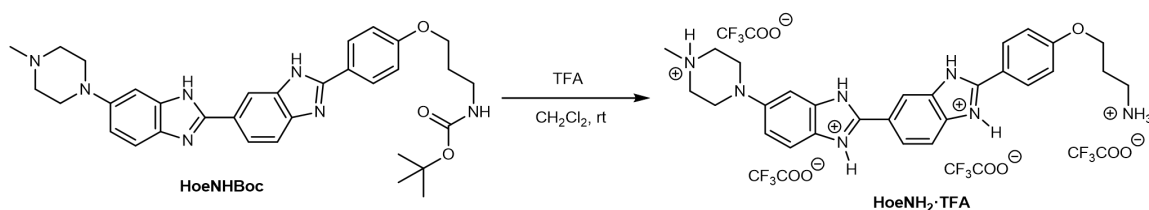


### Procedures for preparation of 6-HoeHESiR

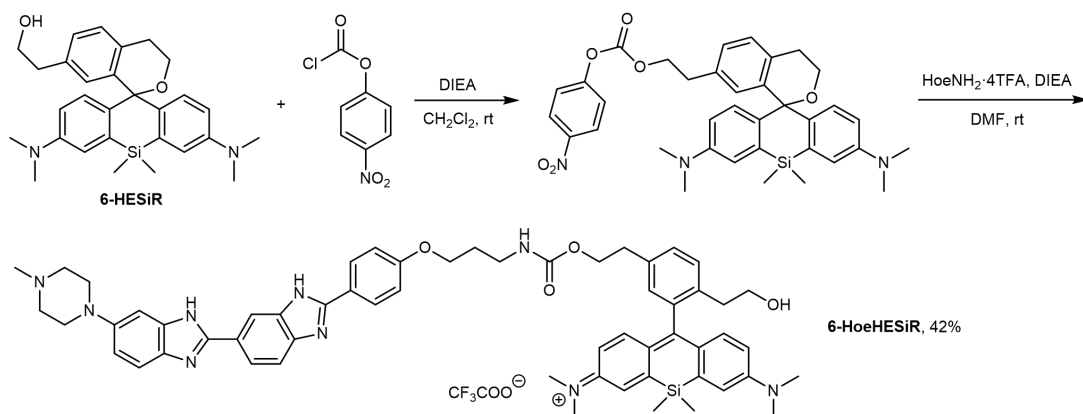


To a 25 mL round-bottom flask with **Hoechst 33258** (63 mg, 0.12 mmol),  $\text{Br}(\text{CH}_2)_3\text{NHBoc}$ <sup>4</sup> (56 mg, 0.236 mmol) and  $\text{K}_2\text{CO}_3$  (49 mg, 0.354 mmol) was added DMF (3 mL). The suspension was stirred vigorously at 60 °C. The reaction mixture was shielded from light with aluminum foil. After two days (reaction time unoptimized), the reaction mixture was cooled to room temperature, diluted with methanol, and filtered. The filtrate was evaporated to dryness and the crude product was purified by flash column chromatography (0% to 10% MeOH/ $\text{CH}_2\text{Cl}_2$ ) to give **HoeNHBOC** as a light yellow solid (42 mg, 0.072 mmol, 61% yield). <sup>1</sup>H NMR (500 MHz,  $\text{CD}_3\text{OD}$ )  $\delta$  8.21 (s, 1H), 8.00 (d,  $J = 8.6$  Hz, 2H), 7.91 (dd,  $J = 8.5, 1.2$  Hz, 1H), 7.65 (d,  $J = 8.4$  Hz, 1H), 7.50 (d,  $J = 8.8$  Hz, 1H), 7.13 (d,  $J$

= 1.8 Hz, 1H), 7.03 (two doublets,  $J = 8.6, 9.6$  Hz, 2H + 1H = 3H), 4.03 (t,  $J = 6.1$  Hz, 2H), 3.29–3.26 (m, 4H), 3.24 (t,  $J = 6.8$  Hz, 2H), 2.93–2.87 (br, 4H), 2.55 (s, 3H), 1.94 (quintet,  $J = 6.5$  Hz, 2H), 1.43 (s, 9H);  $^{13}\text{C}$  NMR (125 MHz,  $\text{CD}_3\text{OD}$ )  $\delta$  162.5, 158.6, 155.3, 153.8, 149.1, 129.5, 125.5, 122.9, 122.5, 116.4, 116.0, 102.6, 80.0, 66.8, 55.8, 51.1, 45.3, 38.4, 30.7, 28.8; HRMS (ESI): calcd for  $\text{C}_{33}\text{H}_{40}\text{N}_7\text{O}_3$  ( $[\text{M} + \text{H}]^+$ ): 582.3187, found: 582.3201.



To a 10 mL round-bottom flask with **HoeNHBOC** (7.9 mg, 0.014 mmol) was added  $\text{CH}_2\text{Cl}_2$  (0.5 mL) and TFA (0.5 mL). The suspension was stirred at room temperature for 1 h 10 min (reaction time unoptimized). Then toluene was added to the flask and the mixture was evaporated to dryness. **HoeNH<sub>2</sub>·4TFA** salt was obtained as a brown oil and was used for the next step without further purification.

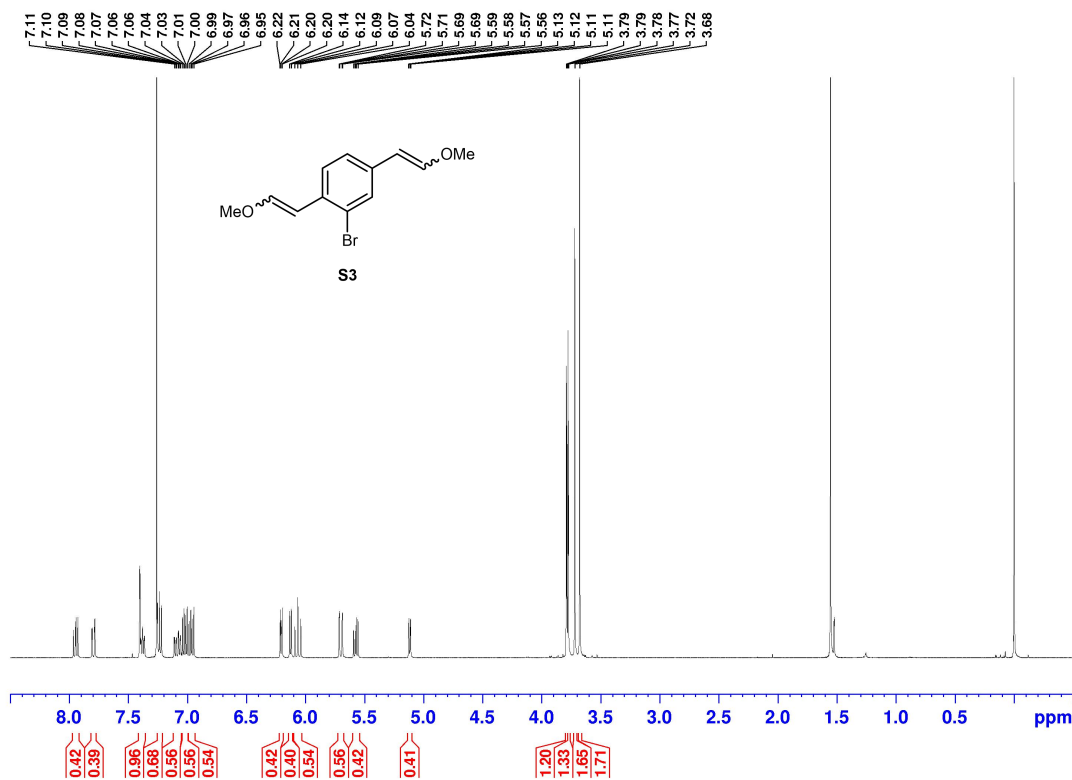


To a 10 mL round-bottom flask with **6-HESiR** (4 mg, 0.009 mmol) was added  $\text{CH}_2\text{Cl}_2$  (0.4 mL) and DIEA (0.1 mL). 4-Nitrophenyl chloroformate (8.5 mg, 0.042 mmol) was added in one portion. The flask was sealed with a septum and stirred at room temperature overnight (reaction time unoptimized). On the next day, the reaction mixture was diluted with EA and quenched with water.

The mixture was stirred vigorously for 15 min and then washed with water and brine. The organic phase was dried over  $\text{MgSO}_4$ , filtered, and concentrated. This mixed carbonate crude product was transferred to a 10 mL round-bottom flask, which was kept under Ar. DMF (anhydrous, 0.5 mL) and DIEA (anhydrous, 0.2 mL) were added to this flask. The resulting solution was added to the 10 mL round-bottom flask with **HoeNH<sub>2</sub>·4TFA** salt under Ar. The first flask with mixed carbonate was rinsed with DMF (anhydrous, 0.3 mL). The reaction mixture was stirred at room temperature overnight under Ar. On the next day, the reaction mixture was passed through a 0.2  $\mu\text{m}$  syringe filter and diluted with water and acetonitrile ( $\text{CH}_3\text{CN}$ ). The crude product was purified by preparative reverse phase HPLC (30% to 70%  $\text{CH}_3\text{CN}/\text{H}_2\text{O}$  with constant 0.1% TFA) to give **6-HoeHESiR** as a deep blue solid (4 mg, 0.004 mmol, 42% yield).  $^1\text{H}$  NMR (500 MHz,  $\text{CD}_3\text{OD}$ )  $\delta$  8.37 (s, 1H), 8.07 (d,  $J = 8.5$  Hz, 2H), 8.00 (d,  $J = 8.4$  Hz, 1H), 7.85 (d,  $J = 8.5$  Hz, 1H), 7.69 (d,  $J = 8.9$  Hz, 1H), 7.42 (AB system,  $J = 8.9, 10.3$  Hz, 2H), 7.37–7.27 (m, 4H), 7.12 (d,  $J = 9.8$ , 2H), 7.10 (d,  $J = 10.5$  Hz, 2H), 7.03 (s, 1H), 6.76 (dd,  $J = 9.5, 1.7$  Hz, 2H), 4.29 (t,  $J = 6.4$  Hz, 2H), 4.06 (t,  $J = 5.8$  Hz, 2H), 3.61–3.48 (br, 4H from the piperazine ring), 3.49 (t,  $J = 7.3$  Hz, 2H), 3.42–3.29 (overlap with NMR solvent peak, 12H of the 4 methyl groups on 2 N atoms of the fluorophore structure), 3.28–3.24 (overlap with NMR solvent peak, 4H from the piperazine ring and 2H from a methylene group of the upper part of the fluorophore structure), 3.01 (s, 3H), 2.98 (t,  $J = 6.2$  Hz, 2H), 2.52 (t,  $J = 7.3$  Hz, 3H), 1.92 (quintet,  $J = 6.2$  Hz, 2H), 0.60 (s, 3H), 0.57 (br, 3H);  $^{13}\text{C}$  NMR (125 MHz,  $\text{CD}_3\text{OD}$ )  $\delta$  171.4, 164.0, 156.6, 151.0, 150.4, 143.7, 141.0, 138.8, 137.1, 132.1, 131.9, 131.6, 130.9, 129.9, 124.1, 122.9, 119.7, 117.2, 116.6, 115.9, 102.6, 67.8, 67.1, 63.8, 55.6, 44.4, 41.7, 39.6, 38.0, 36.9, 31.6, 31.5, 0.8, -0.7; HRMS (ESI): calcd for  $\text{C}_{58}\text{H}_{66}\text{N}_9\text{O}_4\text{Si}$  ( $\text{M}^+$ ): 980.5002, found: 980.5009.

### **$^1\text{H}$ and $^{13}\text{C}$ NMR spectra of new compounds**

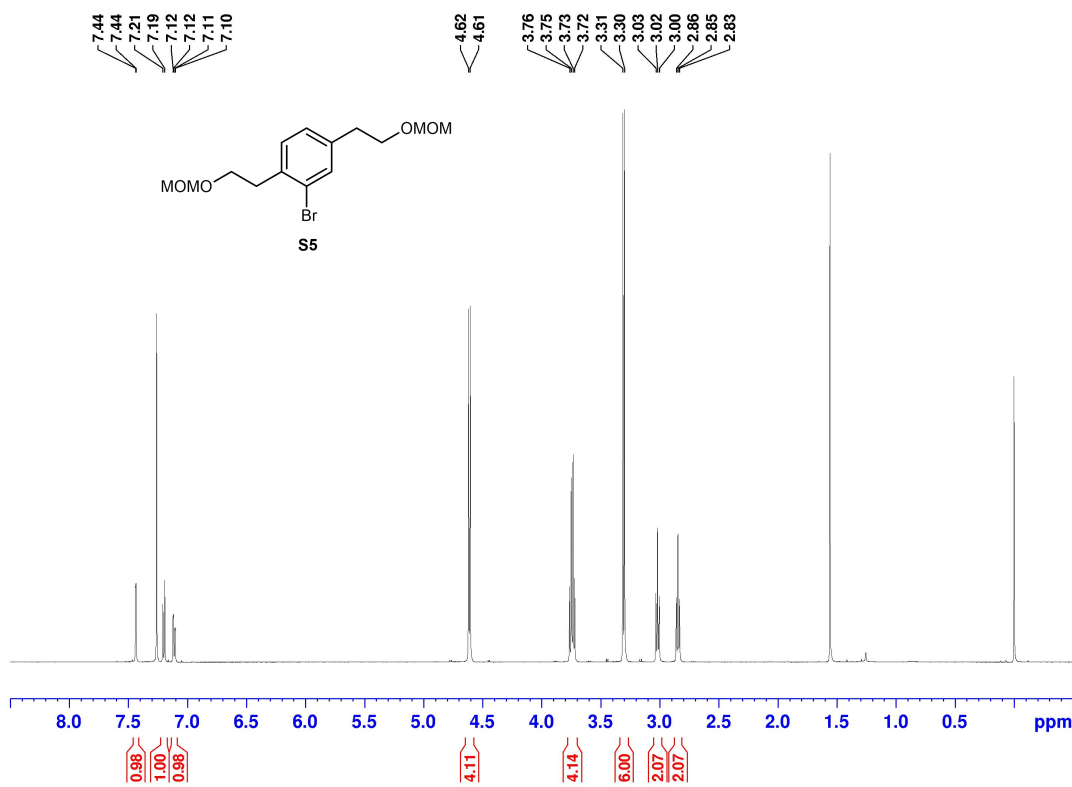




Current Data Parameters  
 NAME yzh-2-52H  
 EXPNO 1  
 PROCNO 1

F2 - Acquisition Parameters  
 Date\_ 20180521  
 Time 15.39 h  
 INSTRUM spect  
 PROBHD Z119470\_0274 (  
 PULPROG zg30  
 TD 32768  
 SOLVENT CDCl3  
 NS 16  
 DS 2  
 SWH 10000.000 Hz  
 FIDRES 0.610352 Hz  
 AQ 1.6384000 sec  
 RG 256  
 DW 50.000 usec  
 DE 6.50 usec  
 TE 296.5 K  
 D1 1.00000000 sec  
 TD0 1  
 SFO1 500.1330883 MHz  
 NUC1 1H  
 P1 8.03 usec  
 PLW1 14.00000000 W

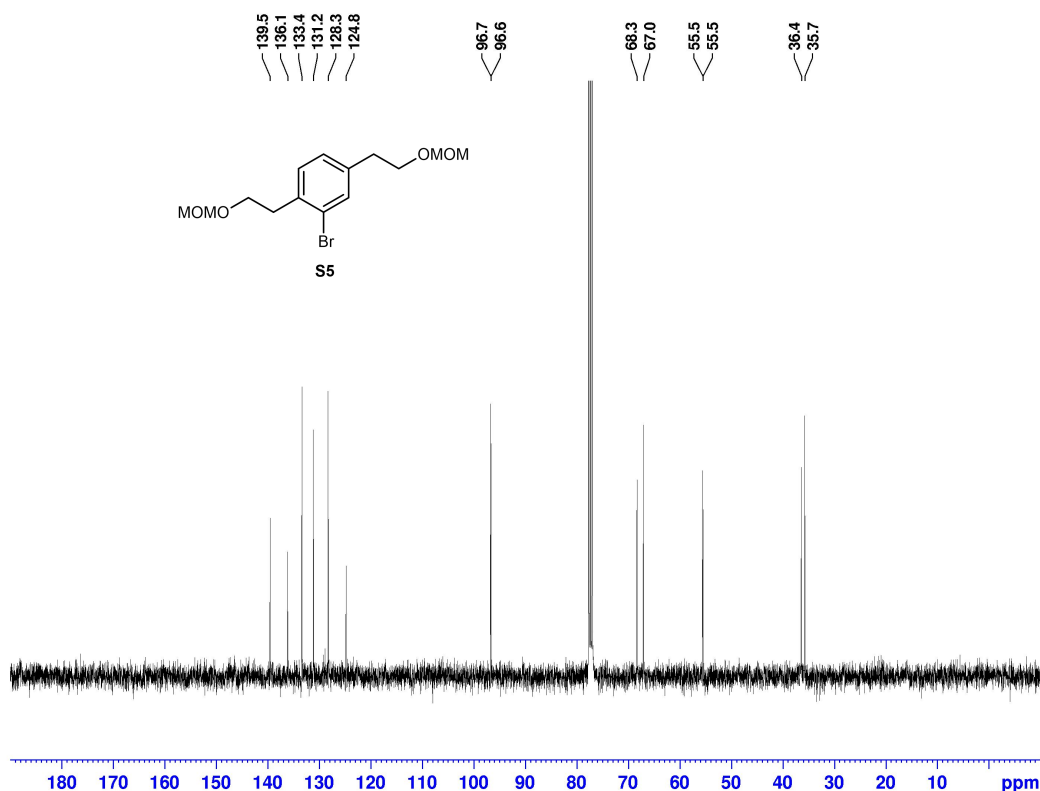
F2 - Processing parameters  
 SI 65536  
 SF 500.1300117 MHz  
 WDW EM  
 SSB 0  
 LB 0.30 Hz  
 GB 0  
 PC 1.00



Current Data Parameters  
 NAME xrq-1-11H  
 EXPNO 1  
 PROCNO 1

F2 - Acquisition Parameters  
 Date\_ 20200508  
 Time 13.47 h  
 INSTRUM spect  
 PROBHD Z119470\_0274 (  
 PULPROG zg30  
 TD 32768  
 SOLVENT CDCl3  
 NS 27  
 DS 2  
 SWH 10000.000 Hz  
 FIDRES 0.610352 Hz  
 AQ 1.6384000 sec  
 RG 256  
 DW 50.000 usec  
 DE 6.50 usec  
 TE 298.0 K  
 D1 1.00000000 sec  
 TD0 1  
 SFO1 500.1330883 MHz  
 NUC1 1H  
 P1 8.03 usec  
 PLW1 14.00000000 W

F2 - Processing parameters  
 SI 65536  
 SF 500.1300120 MHz  
 WDW EM  
 SSB 0  
 LB 0.30 Hz  
 GB 0  
 PC 1.00



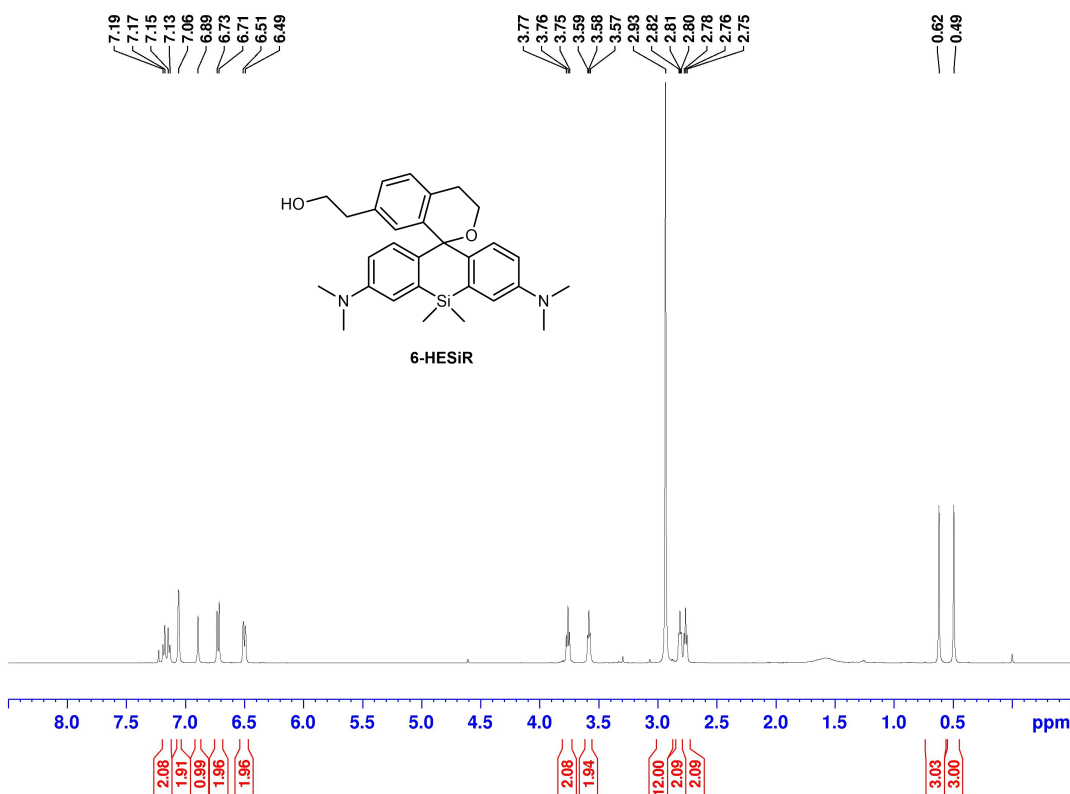
Current Data Parameters  
 NAME yzh-2-99C  
 EXPNO 1  
 PROCNO 1

F2 - Acquisition Parameters  
 Date 20180717  
 Time 10.27  
 INSTRUM spect  
 PROBHD 5 mm QNP 1H/1  
 PULPROG zgdc  
 TD 32768  
 SOLVENT CDCl3  
 NS 201  
 DS 0  
 SWH 25125.629 Hz  
 FIDRES 0.766773 Hz  
 AQ 0.6520832 sec  
 RG 2608  
 DW 19.900 usec  
 DE 20.00 usec  
 TE 0 K  
 D1 2.5000000 sec  
 d11 0.03000000 sec  
 MCREST 0 sec  
 MCWRK 0.01500000 sec

----- CHANNEL f1 -----  
 NUC1 13C  
 P1 9.50 usec  
 PL1 -5.00 dB  
 SFO1 100.6238364 MHz

----- CHANNEL f2 -----  
 CPDPRG2 waltz16  
 NUC2 1H  
 PCPD2 80.00 usec  
 PL2 -4.00 dB  
 PL12 12.90 dB  
 SFO2 400.1320007 MHz

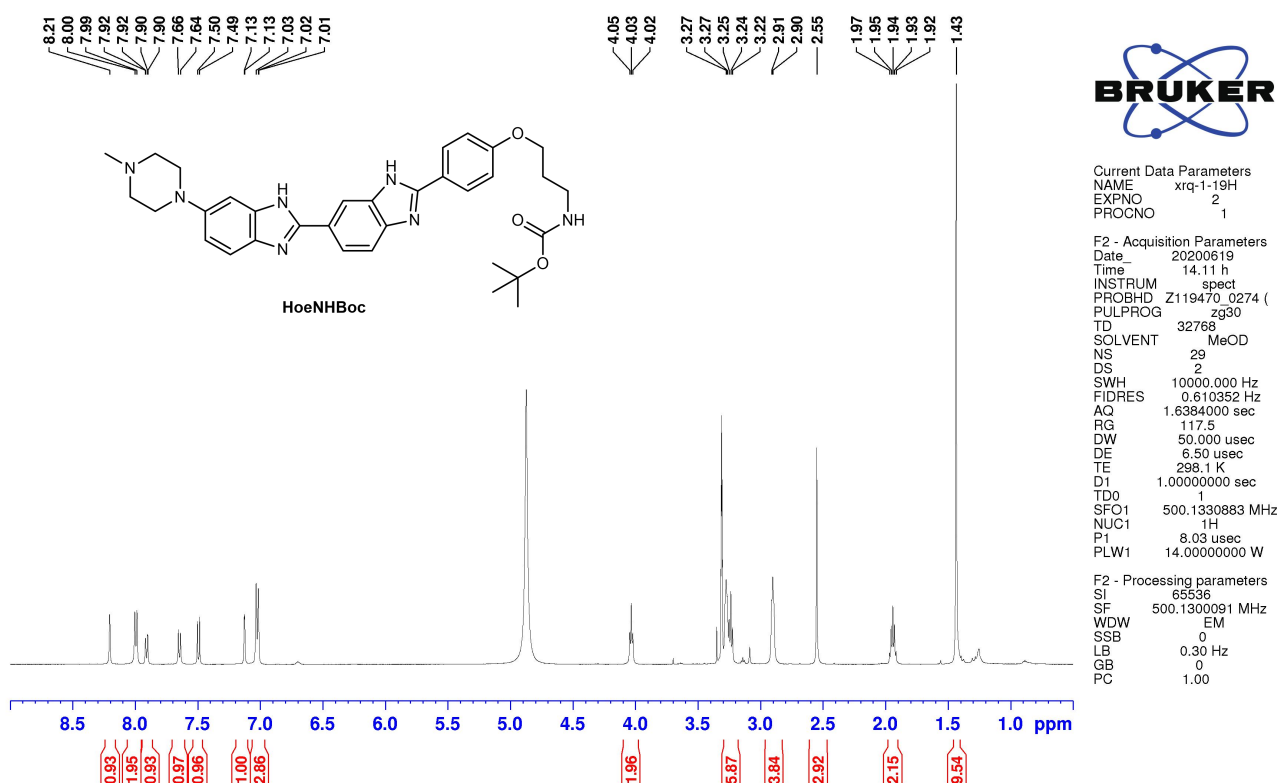
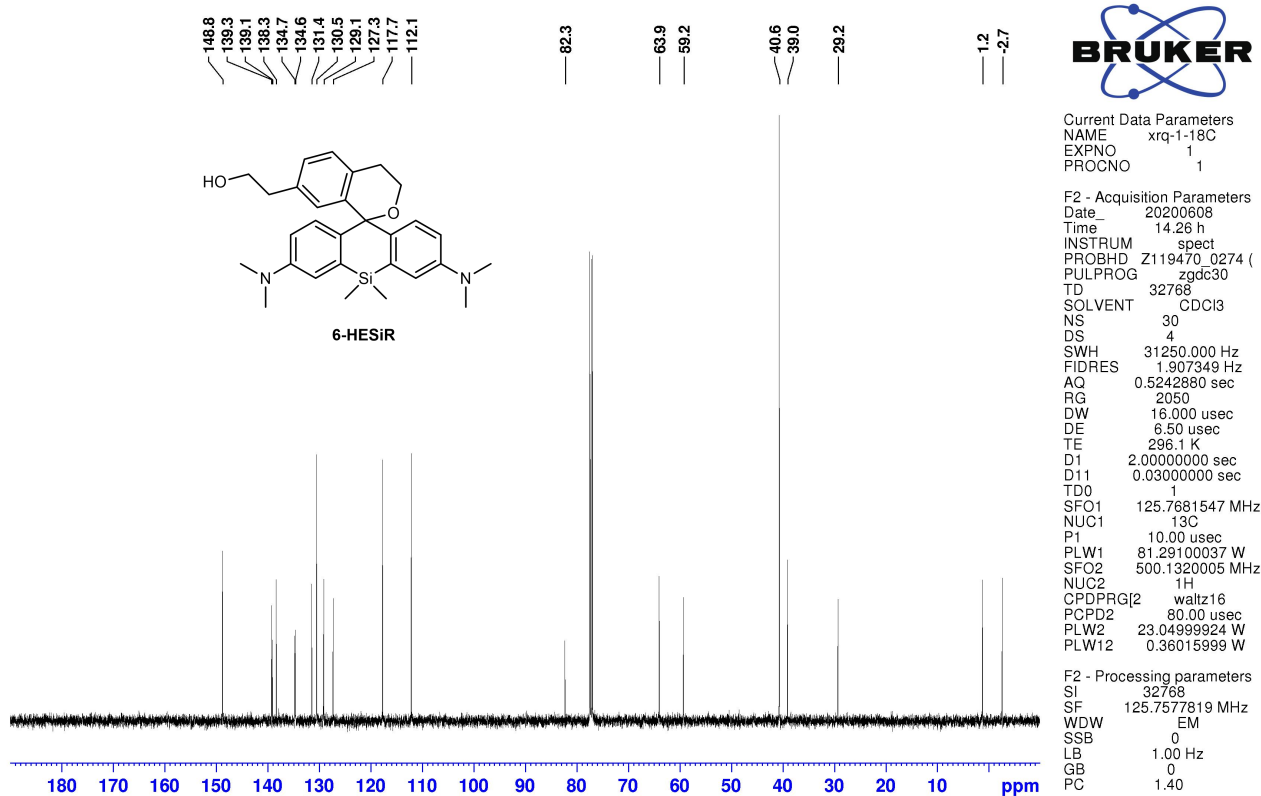
F2 - Processing parameters  
 SI 16384  
 SF 100.6127360 MHz  
 WDW EM  
 SSB 0  
 LB 1.00 Hz  
 GB 0  
 PC 1.40

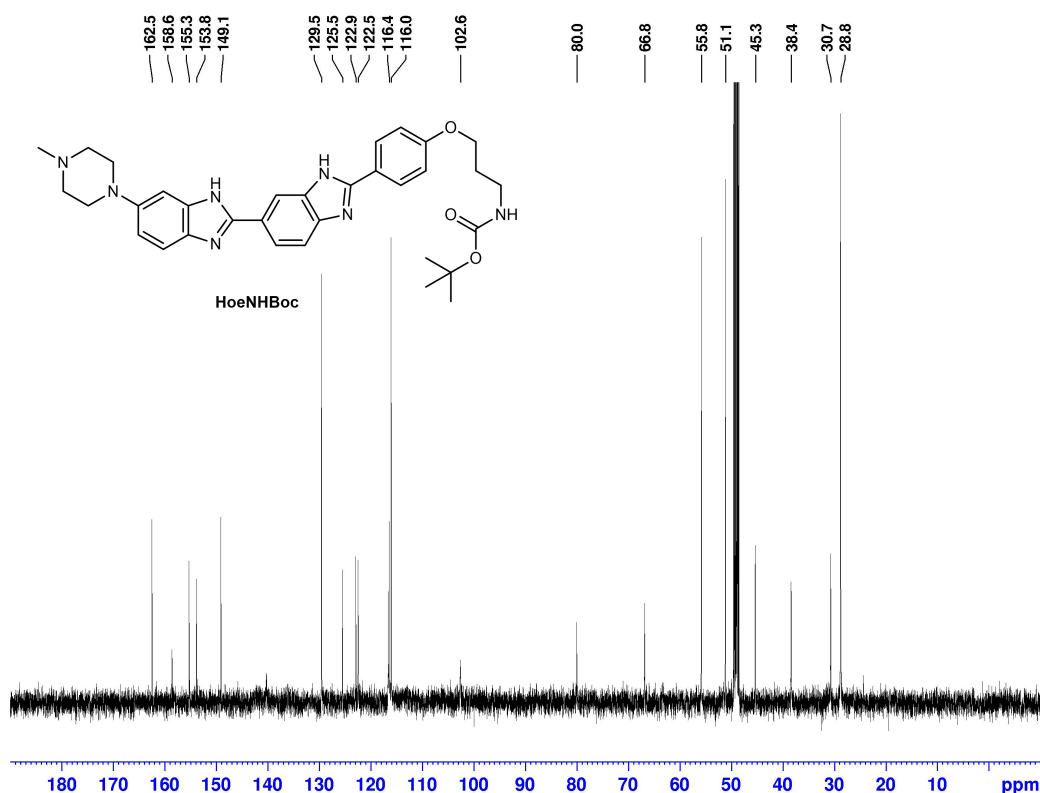


Current Data Parameters  
 NAME xrq-1-18H  
 EXPNO 5  
 PROCNO 1

F2 - Acquisition Parameters  
 Date 20200608  
 Time 13.43 h  
 INSTRUM spect  
 PROBHD Z119470\_0274 (Z  
 PULPROG zg30  
 TD 32768  
 SOLVENT CDCl3  
 NS 32  
 DS 2  
 SWH 10000.000 Hz  
 FIDRES 0.610352 Hz  
 AQ 1.6384000 sec  
 RG 54.39  
 DW 50.000 usec  
 DE 6.50 usec  
 TE 295.4 K  
 D1 1.0000000 sec  
 TD0 1  
 SFO1 500.1330883 MHz  
 NUC1 1H  
 P1 8.03 usec  
 PLW1 14.00000000 W

F2 - Processing parameters  
 SI 65536  
 SF 500.1300291 MHz  
 WDW EM  
 SSB 0  
 LB 0.30 Hz  
 GB 0  
 PC 1.00

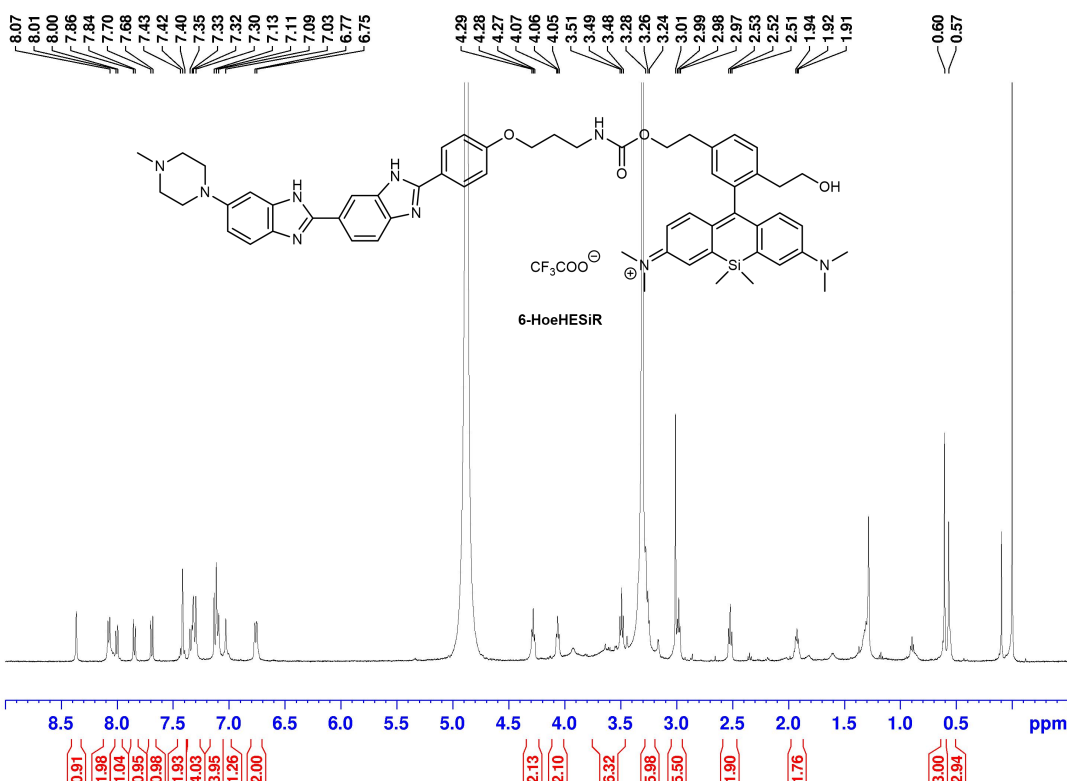




Current Data Parameters  
 NAME xrq-1-19C  
 EXPNO 5  
 PROCNO 1

F2 - Acquisition Parameters  
 Date\_ 20200619  
 Time 16.45 h  
 INSTRUM spect  
 PROBHD Z119470\_0274 (  
 PULPROG zgdc30  
 TD 32768  
 SOLVENT MeOD  
 NS 446  
 DS 4  
 SWH 31250.000 Hz  
 FIDRES 1.907349 Hz  
 AQ 0.5242880 sec  
 RG 2050  
 DW 16.000 usec  
 DE 6.50 usec  
 TE 298.7 K  
 D1 2.00000000 sec  
 D11 0.03000000 sec  
 TD0 1  
 SFO1 125.7681547 MHz  
 NUC1 13C  
 P1 15.00 usec  
 PLW1 96.75700378 W  
 SFO2 500.1320005 MHz  
 NUC2 1H  
 CPDPRG2 waltz16  
 PCPD2 80.00 usec  
 PLW2 14.00000000 W  
 PLW12 0.14266540 W

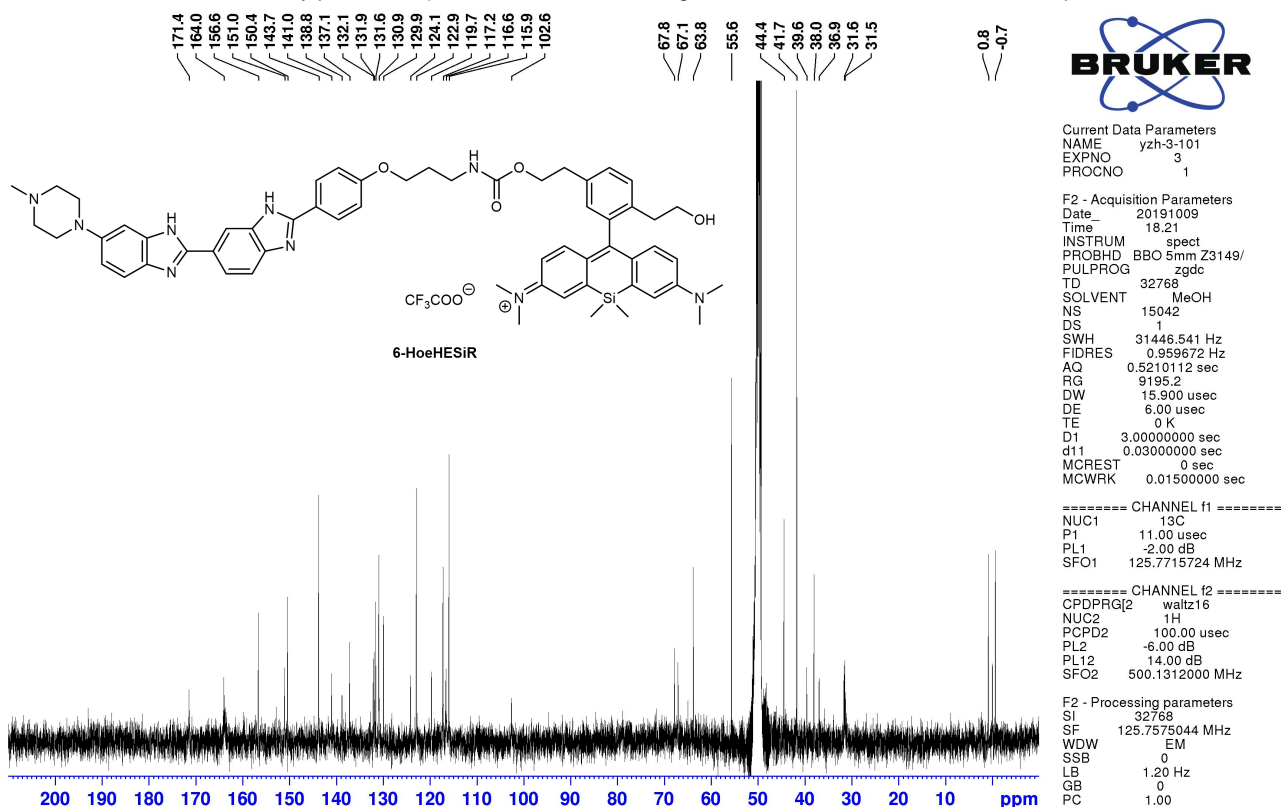
F2 - Processing parameters  
 SI 32768  
 SF 125.7576144 MHz  
 WDW EM  
 SSB 0  
 LB 1.00 Hz  
 GB 0  
 PC 1.40



Current Data Parameters  
 NAME yzh-3-101H  
 EXPNO 3  
 PROCNO 1

F2 - Acquisition Parameters  
 Date\_ 20191009  
 Time 10.44 h  
 INSTRUM spect  
 PROBHD Z119470\_0274 (  
 PULPROG zg30  
 TD 32768  
 SOLVENT MeOD  
 NS 32  
 DS 2  
 SWH 10000.000 Hz  
 FIDRES 0.610352 Hz  
 AQ 1.6384000 sec  
 RG 131.75  
 DW 50.000 usec  
 DE 6.50 usec  
 TE 295.5 K  
 D1 1.00000000 sec  
 TD0 1  
 SFO1 500.1330883 MHz  
 NUC1 1H  
 P1 8.03 usec  
 PLW1 14.00000000 W

F2 - Processing parameters  
 SI 65536  
 SF 500.1300111 MHz  
 WDW EM  
 SSB 0  
 LB 0.30 Hz  
 GB 0  
 PC 1.00



## Materials and methods

### Photophysical properties of 6-HESiR and 6-HoeHESiR

Absorbance was measured on a Shanghai INESA L6S UV-Vis spectrophotometer. Fluorescence emission was measured on an Edinburgh Instruments FS5 Spectrofluorometer. The hpDNA (5'-CGCGAATTCGCGTTTTTCGCGAATTCGCG-3') used for fluorescence titration of **6-HoeHESiR** was purchased from Sangon Biotech. It was prepared by denaturation and annealing in the Tris-HCl buffer (50 mM Tris-HCl, 100 mM NaCl, pH = 7.4) with a digital dry bath. The dsDNA samples used for fluorescence titration studies were prepared from corresponding complementary oligonucleotides (Sangon Biotech) by denaturation and annealing in the same Tris-HCl buffer with a digital dry bath. The fluorescence titration of probe binding sites was performed with 0.5  $\mu$ M **6-HoeHESiR** in the same Tris-HCl saline buffer by sequential addition of the stock solutions of hpDNA and dsDNA.

### Configuration of the microscope for 3D SMLM experiments

All 3D SMLM experiments were performed on a Nano BioImaging SRiS 2.0 STORM Super-resolution Microscope<sup>5</sup> (<https://cpos.hku.hk/imaging-and-flow-cytometry-core/imaging-equipment>; company: INVIEW , <http://www.inview-tech.com>). 3D imaging was performed with astigmatism according to the reported approach<sup>6</sup>. The detailed configuration is listed below.

- Lasers: 647 channel: 656 nm (500 mW); 750 channel: 750 nm (300 mW)
- Microscope base: Nikon eclipse Ti-E
- XY stage: manual manipulator stage, piezo stage insert
- Objective lens: CFI Aopchromat TIRF 100XH, N.A. 1.49, W.D. 0.12 mm, cover glass correction: 0.13-0.21 mm
- 3D lens (for astigmatism):  $f = 1000.0$  mm,  $\varnothing 1$ ", N-BK7 Mounted Plano-Convex Round Cylindrical Lens (LJ1516RM, Thorlabs)
- Detector: Andor iXon Ultra 897 EMCCD Camera; two-channel simultaneous acquisition

with  $320 \times 160$  pixels field of view

- Detection Band (647 channel, 656 nm laser): 672–712 nm (Model: FF01-692/40-25 made by Semrock)
- Dichoric mirror (for splitting between 647 and 750 channel): T760LPXR-UF2 (Chroma Technology Corp.)
- Software: Rohdea 2.0

### **Nucleosome and chromatin reconstitution**

Recombinant histones H2A, H2B, H3, H4 and H1 were cloned and purified as previously described.<sup>7</sup> Reconstitution of histone octamers were performed as described previously.<sup>8</sup> Equimolar amounts of individual histones in unfolding buffer (7 M guanidinium HCl, 20 mM Tris-HCl, pH 7.5, 10 mM DTT) were dialyzed into refolding buffer (2 M NaCl, 10 mM Tris-HCl, pH 7.5, 1 mM EDTA, 5 mM 2-mercaptoethanol), and purified using Superdex S200 column. DNA templates of the 40–187bp DNA were cloned and purified as previously described.<sup>8</sup> Two single-stranded overhangs of DNA templates digested by BseYI enzyme were labeled with either dUTP-digoxigenin or dATP-biotin by Klenow reaction. Nucleosome samples were assembled using the salt-dialysis method as previously described.<sup>8</sup> Equimolar amounts of histone octamers and 40-187bp DNA templates were mixed in TEN buffers (10 mM Tris-HCl, pH 8.0, 1 mM EDTA, 2 M NaCl) and dialyzed for 17 hrs at 4 °C in TEN buffer, which was continuously diluted by slowly pumping in TE buffer (10 mM Tris-HCl, pH 8.0, 1mM EDTA) to lower concentration of NaCl from 2 M to 0.6 M. For histone H1 incorporation, histone H1 was added at this step and further dialyzed for 3 h. Samples were collected after final dialysis in HE buffer (10 mM HEPES, pH 8.0, 1 mM EDTA) for 4 h.

### **Electron microscopy analysis**

Metal shadowing with tungsten for EM study was performed as described previously.<sup>9</sup> Reconstituted

nucleosome samples (2 ng/ $\mu$ l) were fixed with 0.4% glutaraldehyde in HE buffer on ice for 30 min.

After 2 mM spermidine was added, samples were applied to glow-discharged carbon-coated EM grids and incubated for 2 min and then blotted. Grids were washed stepwise in 0%, 25%, 50%, 75%, and 100% ethanol solution for 4 min at room temperature, air dried and shadowed with tungsten at an angle of 10° with rotation. For the negative staining, the chromatin samples in fixative solution were incubated on glow-discharged carbon-coated EM grids for 1 min. The excess sample solution was removed using filter papers. The grid was incubated in 2% Uranylacetate for staining for 30 s twice, blotted with filter papers and allowed to air-dry for several minutes. The prepared EM samples were examined using a FEI Tecnai G2 Spirit 120 kV transmission electron microscope.

### **SMLM with spin-coated lambda DNA**

Lambda DNA (ThermoFisher, SD0011) was dissolved in 1 × TE50 buffer (pH = 7.5) to a concentration of 0.4  $\mu$ g/mL and the solution was stored at 4 °C. The stock solution of **6-HoeHESiR** was diluted in ddH<sub>2</sub>O to the concentration of 0.1  $\mu$ M and the solution was stored at 4 °C. A confocal dish (cellvis, D35-10-1-N) was incubated with 0.1 mg/mL poly-L-lysine (Sigma) for 1 h. Then the well in the dish was washed with ddH<sub>2</sub>O three times and air-dried. The dish was fixed onto a spin-coater. The solution of lambda DNA (100  $\mu$ L) was added to the dish. After 20 s of settling down, the spin speed was adjusted to 4000 rpm and kept for 60 s. During the spinning process, 2 mL ddH<sub>2</sub>O was added. After spin-coating, the solution of **6-HoeHESiR** (100  $\mu$ L) was added to the dish for imaging. SMLM experiment was carried out on a home-built microscope with an Olympus IX73 base, a 100× NA = 1.5 oil-immersion objective and an Andor iXon897 EMCCD camera. 10,000 frames were acquired with laser intensity of 3.5 kW/cm<sup>2</sup> at 671 nm, 50 ms camera exposure, and EM gain of 30.

### **3D SMLM of reconstituted nucleosomal arrays and 30-nm chromatin fibers**



A sample of *in vitro* reconstructed 30-nm chromatin fibers ( $40 \times 187$  bp with H1 and biotin label) and a sample of *in vitro* reconstructed nucleosomal arrays ( $40 \times 187$  bp without H1) were prepared. Streptavidin (1 mg, Sigma Aldrich, S4762-1MG) was dissolved in 1 mL PBS (1 mg/mL). 5  $\mu$ L of this stock solution was diluted in 400  $\mu$ L MQ water. In a 35 mm culture dish (Corning), this diluted solution was loaded onto an 18 mm round coverslip (Marienfeld precision cover glass thickness No. 1.5H) which has been sequentially coated with 3  $\mu$ m microbeads (Sigma Aldrich, 79166-5ML-F) and poly-D-lysine (Sigma Aldrich, P0899-50MG, MW = 70,000–150,000). After 10 min, the solution was removed, and the coverslip was washed with MQ water. The sample of reconstructed 30-nm chromatin fibers (2.5  $\mu$ L, 63.1 ng/ $\mu$ L) was added to 400  $\mu$ L HE buffer (10 mM HEPES, 1 mM EDTA, pH = 7.5) containing 2.5  $\mu$ M **6-HoeHESiR**. The resulting solution was loaded onto the coverslip with immobilized streptavidin. After 10 min, the solution was replaced with 380  $\mu$ L HE buffer. 3D SMLM of reconstituted 30-nm chromatin fibers was carried out in HE buffer at room temperature by applying 950 W/cm<sup>2</sup> excitation laser intensity at 656 nm. Exposure time of EMCCD camera was 17.7 ms/frame. 5,000 frames were acquired for each field of view. The sample of reconstituted nucleosomal arrays (1  $\mu$ L, 69 ng/ $\mu$ L) was added to 400  $\mu$ L HE buffer containing 2.5  $\mu$ M **6-HoeHESiR**. The resulting solution was loaded onto the coverslip coated with poly-D-lysine. After 10 min, the solution was replaced with 380  $\mu$ L HE buffer. 3D SMLM of reconstituted nucleosomal arrays was carried out in HE buffer at room temperature using the same set of imaging parameters. Real-time drift correction was applied by the active locking function of Rohdea software using the microbeads coated on coverslip.

### **Light-sheet microscopy of living HeLa cells**

HeLa cells were cultured in DMEM (Dulbecco's Modified Eagle Medium, Gibco) supplemented with phenol red, 10% heat-inactivated fetal bovine serum (Gibco) and 1% penicillin/streptomycin (Gibco), at 37 °C with 5% CO<sub>2</sub>. 5 mm coverslips (provided by Light Innovation Technology Ltd.)

were sonicated in 75% ethanol for 10 min, air-dried and placed in a 35 mm culture dish. Cells were typically seeded at a density of 0.5 or  $1 \times 10^5$  cells/mL the day before imaging. On the day of imaging, HeLa cells were incubated with **6-HoeHESiR** (5  $\mu$ M for 30 min) and **6-HESiR** (2  $\mu$ M for 30 min) in 1 mL DMEM at 37 °C with 5% CO<sub>2</sub>. The cells were washed with DMEM once and placed back to the incubator with 1 mL DMEM in the dish. After 30 min, the cells were washed with DMEM once or twice before imaging. A coverslip with stained cells was placed in a sample holder and mounted. Live-cell 3D imaging was carried out in DMEM at 37 °C with 647-nm excitation laser and 30-ms camera exposure using a light-sheet microscope (Light Innovation Technology Ltd., [LiTone LBS Light-sheet Microscope | litsite](#)).

### **Cytotoxicity assay**

HeLa cells were seeded in a 96-well plate at a density of 5000 cells/well and cultured in DMEM supplemented with phenol red, 10% heat-inactivated fetal bovine serum, 1% penicillin/streptomycin, and various concentrations of **6-HoeHESiR** at 37 °C with 5% CO<sub>2</sub>. After 3 h, 10  $\mu$ L of WST-1 reagent (Beyotime, C0036) was added to each well. After another 2 h, the absorbance readouts of each well were measured at 450 and 690 nm with a microplate reader (Thermo Varioskan LUX). Cell viability (%) data were obtained based on corrected absorbance values and a calibration curve of absorbance versus cell density.

### **3D SMLM of living HeLa cells**

HeLa cells were cultured in DMEM supplemented with phenol red, 10% heat-inactivated fetal bovine serum and 1% penicillin/streptomycin, at 37 °C with 5% CO<sub>2</sub>. A UV sterilized 18 mm round coverslip coated with 3  $\mu$ m was placed in a 35-mm culture dish with coated face up. Cells were typically seeded at a density of 0.5 or  $1 \times 10^5$  cells/mL the day before imaging. On the day of imaging, HeLa cells were incubated with 5  $\mu$ M **6-HoeHESiR** for 30 min in 1 mL DMEM at 37 °C

with 5% CO<sub>2</sub>. The cells were washed with DMEM and placed back to the incubator with 1 mL DMEM in the dish. After 15–20 min, the cells were washed with DMEM before imaging. Live-cell 3D SMLM was carried out in 380 µL DMEM at room temperature by applying 3.2 kW/cm<sup>2</sup> or 950 W/cm<sup>2</sup> excitation laser intensity at 656 nm. Exposure time of EMCCD camera was 17.7 ms/frame. 5,000 frames were acquired for each field of view. Real-time drift correction was applied by the active locking function of Rohdea software using the microbeads coated on coverslip.

For treatments with HDAC inhibitors, HeLa cells were seeded on the day before imaging. Cells were treated with 200 nM TSA, 2 µM entinostat, and 1 µM ricolinostat for 20 h in DMEM, respectively. On the day of imaging, 3D SMLM experiments were carried out with the same experimental procedure and parameters as untreated cells.

### **3D SMLM of living chicken erythrocytes**

20 µL chicken erythrocyte cell suspension (Innovative Research, 5% solution in Alsever's) was added to 1 mL DMEM containing 0.5 µM **6-HoeHESiR**. The suspended cells were incubated for 10 min in DMEM at 37 °C with 5% CO<sub>2</sub>. The cells were centrifuged and DMEM was removed. Cells were washed with 1 mL HBSS (Hanks' Balanced Salt solution) and resuspended in 200 µL HBSS. The suspended cells in HBSS were loaded onto a microbead-coated coverslip having immobilized poly-D-lysine. The cells were allowed to settle down and attach to the coverslip for 5–10 min. Then the cell suspension was replaced with 380 µL HBSS. Live-cell 3D SMLM was carried out in HBSS at room temperature by applying 950 W/cm<sup>2</sup> excitation laser intensity at 656 nm. Exposure time of EMCCD camera was 17.7 ms/frame. 10,000 frames were acquired for each field of view. Real-time drift correction was applied by the active locking function of the Rohdea software using the microbeads coated on coverslip.

### **Chromatin image data analysis**

Super-resolved images were generated by FIJI<sup>10</sup> with ThunderSTORM<sup>11</sup> plugin using “Normalized Gaussian” reconstruction algorithm. The result table of acquired localizations for each field of view was generated by the Rohdea software and directly used for chromatin image data analysis. Magnification ratio is set as 10.6 to give a 10-nm pixel size in reconstructed images. Original pixel size is 106 nm and original field of view is 320 pixel (width) × 160 pixel (height). Axial position (nm) is represented by RGB color depth coding. Axial range is set as -500 to 500 nm. XZ and YZ 3D projection images of representative chromatin fibers were generated by the chromatin fiber analysis program and by Volume Viewer plugin in FIJI (orange hot pseudo-color). Blinking and time-lapse videos were produced by FIJI. 3D rotation videos of representative chromatin fibers were produced by Volume Viewer plugin in FIJI (orange hot pseudo-color).

We have developed a computer program for quantitative analysis of chromatin fibers. The program performs automated analysis of molecular clusters as potential chromatin fibers based on a set of user-defined parameters. The source code of the computer program is available at <https://github.com/HKU-BAL/Chromatin-Fiber-Imaging>. The flowchart of the analysis is presented in Supplementary Fig. 12. The program takes in an input table that contains “the coordinates of localized single molecules”, “localization precision”, “photon count”, and “frame number”. First, the input data is processed by a preprocessing module, which is applied for: 1) filtering out the imprecise localizations with the precision threshold set as 30 nm; 2) magnifying the X and Y coordinates with the ratio of 10.6; 3) grouping the single molecules based on Z-coordinates into 10 nm per slice; and 4) split the data table into 250 or 500 frames a group for ease of analysis. Second, the XY projection image of one frame interval data table is rendered by the “average shifted histogram” algorithm with lateral shift set as 2 and axis shift set as 4. The localized single molecules are assigned to respective clusters according to their 8-way pixel connectivity in the X and Y-axes. A noise removal module that applies the “gray value thresholding strategy” and “outlier Z slice removing by max z gap tolerance” is used. To preserve maximum information, for each instance, both the original cluster

and the cluster after noise removal are kept for subsequent analyses. In the end, the XY, YZ, and XZ projection images of the identified clusters are rendered. For the identification of chromatin fibers with sufficient resolution and labeling density, we set up the following criteria: 1) continuous fibrous structure in YZ and XZ projection images; 2) number of localizations  $\geq 10$ , resulting in labeling density  $\geq 18,000$  molecules/ $\mu\text{m}^3$ ; 3) localization precision threshold of 15 nm; 4) maximum frame gap  $\leq 40$  frames; 5) maximum Z gap  $\leq 50$  nm. Long fiber diameter was the larger lateral FWHM value for each identified fiber. Short fiber diameter was the smaller lateral FWHM value for each identified fiber. Labeling density was calculated by the number of localizations for a chromatin fiber divided by its volume. The volume of a fiber is calculated by the total number of pixel cubes times the volume of each pixel cube, which is  $10^{-6} \mu\text{m}^3$ . The resting/dwelling lifetime of a chromatin fiber was calculated by camera exposure 17.7 ms times the number of frames in which the localizations for that fiber were acquired.

The lateral and axial dimensions of a molecular cluster (a potential chromatin fiber) are estimated based on full width at half maximum (FWHM). To avoid potential bias in calculating FWHM, we adopted a “moving line” strategy. Using the estimation of the X dimension as an example, the process is illustrated in Supplementary Fig. 13a. The line moves on the cluster at the positions that cover the pixels at both the left and the right ends. The line width is set from 1 to the maximum that covers the whole cluster. Additionally, lines with too large FWHM fitting errors are discarded. The threshold is set as 6 for lateral FWHM and 30 for axial FWHM. The gray value submatrix within the line can be formulated as:

$$G_r = \begin{pmatrix} g_{i,j} & \cdots & g_{i,j+L} \\ \vdots & \ddots & \vdots \\ g_{i+w,j} & \cdots & g_{i+w,j+L} \end{pmatrix} \quad (1)$$

where  $w$  denotes the line width.  $L$  denotes the number of pixels horizontally of the cluster.  $i, j$  represents the upper left position of the cluster.  $g_{i,j}$  denotes the gray value at the position  $(i,j)$

Then, the data points (X, Y) can be presented as:

$$\mathbf{X} = (x_0, x_1, \dots, x_L) \quad (2)$$

$$x_k = (k - i) * a \quad (3)$$

$$\mathbf{Y} = (y_0, y_1, \dots, y_L) \quad (4)$$

$$y_k = \frac{\sum_{v=0}^w g_{i+v,k}}{w} \quad (5)$$

where  $x_k$  denotes the distance between the  $k^{\text{th}}$  position and the most left position of the line.  $a$  represents the size of one pixel in the nanometer scale, which is 10 in this study.  $y_k$  denotes the normalized gray value at  $x_k$ .

The FWHM of a molecular cluster is estimated by fitting a Gaussian curve:

$$y = y_0 + Ae^{-\frac{(x-x_c)^2}{2\omega^2}} \quad (6)$$

The parameters are initiated by:

$$y_0 = \min(\mathbf{Y}) \quad (7)$$

$$A = \max(\mathbf{Y}) - \min(\mathbf{Y}) \quad (8)$$

$$x_c = \mathbf{X}_{\text{argmax}(\mathbf{Y})} \quad (9)$$

$$\omega = \text{std}(\mathbf{X}) \quad (10)$$

Then, the curve fitting is optimized by the Levenberg-Marquardt algorithm.

Finally:

$$FWHM = 2\sqrt{2\ln 2}\omega \quad (11)$$

$$FWHM_{err} = 2\sqrt{2\ln 2}\omega_{err}$$

The FWHM values are presented in two ways: 1) mean FWHM of all the lines, and 2) the FWHM with maximum line width.

To reduce potential “noise” signals close to the molecular clusters that might interfere with subsequent analysis, a “noise” removal module is utilized. The module consists of a “gray value thresholding” strategy and an “the outlier Z slice removing by max z gap tolerance” strategy (Supplementary information, Fig. 13b). The gray value thresholding is applied to XY, YZ and XZ

projections of an identified molecule cluster. The key principle is “divide and conquer”. By removing the low gray value pixels, a large, connected cluster can be split into several smaller connected components and these components are analyzed by following the same process as the original cluster. On the other hand, the basic idea of the outlier Z slice removing strategy is to detect and discard the top and/or bottom localizations which are separated from nearest neighboring localizations by Z gaps.

### **Quantification and statistical analysis**

Quantification and statistical analysis were performed with Microsoft Excel and Graphpad Prism 9.

Statistical graphs were generated with Graphpad Prism 9.

## References

1. Ohtake, Y. *et al.* Discovery of Tofogliflozin, a Novel C-Arylglucoside with an O-Spiroketal Ring System, as a Highly Selective Sodium Glucose Cotransporter 2 (SGLT2) Inhibitor for the Treatment of Type 2 Diabetes. *J. Med. Chem.* **55**, 7828-7840 (2012).
2. Xie, Z., Yoon, S.-J. & Park, S. Y. Synthesis of Highly Fluorescent and Soluble 1,2,4-Linking Hyperbranched Poly(arylenevinylene) Featuring Intramolecular Energy Funneling. *Adv. Funct. Mater.* **20**, 1638-1644 (2010).
3. Butkevich, A. N., Lukinavičius, G., D'Este, E. & Hell, S. W. Cell-Permeant Large Stokes Shift Dyes for Transfection-Free Multicolor Nanoscopy. *J. Am. Chem. Soc.* **139**, 12378-12381 (2017).
4. Fang, L. *et al.* Chemoproteomic Method for Profiling Inhibitor-Bound Kinase Complexes. *J. Am. Chem. Soc.* **141**, 11912-11922 (2019).
5. Huang, B., Wang, W., Bates, M. & Zhuang, X. Three-Dimensional Super-Resolution Imaging by Stochastic Optical Reconstruction Microscopy. *Science* **319**, 810-813 (2008).
6. Luger, K., Mäder, A. W., Richmond, R. K., Sargent, D. F. & Richmond, T. J. Crystal structure of the nucleosome core particle at 2.8 Å resolution. *Nature* **389**, 251-260 (1997).
7. Chen, P. *et al.* H3.3 actively marks enhancers and primes gene transcription via opening higher-ordered chromatin. *Genes Dev.* **27**, 2109-2124 (2013).
8. Li, W. *et al.* FACT Remodels the Tetranucleosomal Unit of Chromatin Fibers for Gene Transcription. *Mol. Cell* **64**, 120-133 (2016).
9. Zhao, T. *et al.* A user-friendly two-color super-resolution localization microscope. *Opt. Express* **23**, 1879-1887 (2015).
10. Schindelin, J. *et al.* Fiji: an open-source platform for biological-image analysis. *Nat. Methods* **9**, 676-682 (2012).



11. Ovesný, M., Křížek, P., Borkovec, J., Švindrych, Z. & Hagen, G. M. ThunderSTORM: a comprehensive ImageJ plug-in for PALM and STORM data analysis and super-resolution imaging. *Bioinformatics* **30**, 2389-2390 (2014).